Article

SOURCE DATA | TRANSPARENT PROCESS

THE EMBO JOURNAL

MIWI prevents aneuploidy during meiosis by cleaving excess satellite RNA

Chia-Ling Hsieh, Jing Xia & Haifan Lin*

Abstract

MIWI, a murine member of PIWI proteins mostly expressed during male meiosis, is crucial for piRNA biogenesis, post-transcriptional regulation, and spermiogenesis. However, its meiotic function remains unknown. Here, we report that MIWI deficiency alters meiotic kinetochore assembly, significantly increases chromosome misalignment at the meiosis metaphase I plate, and causes chromosome mis-segregation. Consequently, *Miwi*-deficient mice show elevated aneuploidy in metaphase II and spermatid death. Furthermore, in *Miwi*-null and *Miwi* slicer-deficient mutants, major and minor satellite RNAs from centromeric and pericentromeric satellite repeats accumulate in excess. Over-expression of satellite repeats in wild-type spermatocytes also causes elevated chromosome misalignment, whereas reduction of both strands of major or minor satellite RNAs results in lower frequencies of chromosome misalignment. We show that MIWI, guided by piRNA, cleaves major satellite RNAs, generating RNA fragments that may form substrates for subsequent Dicer cleavage. Furthermore, Dicer cleaves all satellite RNAs in conjunction with MIWI. These findings reveal a novel mechanism in which MIWI- and Dicer-mediated cleavage of the satellite RNAs prevents the over-expression of satellite RNAs, thus ensuring proper kinetochore assembly and faithful chromosome segregation during meiosis.

Keywords PIWI; dicer; meiosis; satellite transcript; aneuploidy
Subject Category RNA Biology
DOI 10.15252/embj.2019103614 | Received 2 October 2019 | Revised 10 June 2020 | Accepted 16 June 2020 | Published online 17 July 2020
The EMBO Journal (2020) 39: e103614

Introduction

Meiosis produces haploid gametes from a diploid parental cell by two sequential rounds of cell division, known as meiosis I and meiosis II, following a single round of DNA replication. The reduction of the chromosome number in meiosis ensures constant ploidy throughout generations. Faithful meiotic segregation of chromosomes is critical for normal reproduction and gamete quality. Chromosome segregation defects in either meiosis I or meiosis II contribute to gametic loss, reduced fertility, and aneuploidy (Potapova & Gorbsky, 2017). As in mitosis, the key regulator of chromosome segregation in meiosis is the spindle assembly checkpoint, a cell surveillance pathway that avoids precocious anaphase onset until all kinetochores correctly connect chromosomes to spindle microtubules (Gorbsky, 2015). Upon prolonged spindle damage, cells induce strong metaphase arrest and eventually undergo apoptosis (Hain *et al*, 2016). Thus, understanding the mechanism underlying the formation of kinetochore–microtubule attachment and accurate chromosome segregation can provide insights into aneuploidy and sterility.

The kinetochore is a proteinaceous complex composed of the inner plate that adheres to centromeric chromatin and the outer plate that binds to microtubules and facilitates proper chromosome alignment (Yamagishi *et al*, 2014). During meiosis I, sister kinetochores are fused or juxtaposed side-by-side and thus attach to microtubules in a syntelic manner. This is in contrast to the amphitelic attachment in mitosis and meiosis II, which resolves sister kinetochores from opposite poles. These distinct kinetochore geometries of mitotic and meiotic chromosomes are determined by sister chromatid cohesions within centromeres (Watanabe, 2012). Like yeast, the molecular architecture of kinetochore and establishment of cohesion in mammals relies on two chromatin domains: centromeric chromatin that incorporates a conserved specialized histone H3 variant called centromere protein A (CENP-A) to form a kinetochore-assembling core, and pericentromeric heterochromatin that flanks centromeric chromatin and contains a high density of cohesin to mediate sister-chromatin cohesion (Allshire & Karpen, 2008). DNA corresponding to centromeric and pericentromere regions consists of extensive arrays of tandem repeats termed minor satellite (120-bp repeats) and major satellites (234-bp repeats), respectively (Wong & Rattner, 1988; Joseph *et al*, 1989; Vissel & Choo, 1989). These areas of the genome are transcriptionally active across species (Chen *et al*, 2008; Eymery *et al*, 2009b; Moazed, 2009). In mammalian somatic cells, the centromere- and pericentromere-derived non-coding RNA transcripts serve as a critical determinant in the formation of the centromere and associated chromatin structure via an elaborate interplay between epigenetic and RNAi-dependent mechanisms, which entails Dicer-mediated RNA processing and RNA-facilitated heterochromatin assembly (Fukagawa *et al*, 2004; Kanellopoulou *et al*, 2005; Murchison *et al*, 2005; Huang *et al*, 2015). These RNA species appear to be crucial for the assembly of the centromere and the kinetochore as well as for the cohesion of sister chromatids, since slight changes in expression of these RNAs or defects in

Yale Stem Cell Center and Department of Cell Biology, Yale University School of Medicine, New Haven, CT, USA
*Corresponding author. Tel: +1 203 785 6239; E-mail: haifan.lin@yale.edu

their turnover lead to mis-localization of centromere proteins, chromosome mis-segregation, chromosome instability, and aneuploidy (Bouzinba-Segard *et al*, 2006; Eymery *et al*, 2009b; Ting *et al*, 2011; De La Fuente *et al*, 2015; Kishikawa *et al*, 2016). In line with this, Dicer has been implicated in the regulation of pericentromere-derived major satellite transcripts in meiosis (Khalil & Driscoll, 2010; Korhonen *et al*, 2011). However, it remains elusive what other factors are possibly involved in the regulation of centromere- and pericentromere-derived transcripts during meiosis and how they regulate meiosis.

PIWI proteins are a subfamily of the AGO/PIWI protein family. PIWI proteins mainly exist in germ cells and associate with PIWI-interacting RNAs (piRNAs), a class of 24–31-nt PIWI-binding small non-coding RNAs (Thomson & Lin, 2009). In mice, the three PIWI proteins, MILI, MIWI, and MIWI2, are expressed during different stages of male germ cell differentiation and are required for spermatogenesis (Deng & Lin, 2002; Ernst *et al*, 2017). MIWI2 is expressed in perinatal germ cells immediately prior to the initiation of spermatogenesis (Aravin *et al*, 2008), whereas MILI is present from the fetal germ cell stage up to the round spermatid stage (Zheng & Wang, 2012). MIWI is only expressed in adolescent and adult testes, from mid-pachytene spermatocytes to early elongating spermatids (Deng & Lin, 2002). In parallel, male germ cells express two developmentally distinct populations of piRNAs, termed pre-pachytene (also known as prospermatogonial) and pachytene piRNAs, respectively (Grivna *et al*, 2006a; Aravin *et al*, 2007). Pre-pachytene piRNAs are predominantly derived from transposable elements in fetal and perinatal male germ cells. They bind to MILI and MIWI2 and participate in silencing of transposons at both epigenetic and post-transcriptional levels (Aravin *et al*, 2008; Kuramochi-Miyagawa *et al*, 2008; Kojima-Kita *et al*, 2016). On the other hand, pachytene piRNAs are mainly transcribed from piRNA clusters in later spermatocytes and post-meiotic spermatids. They mostly associate with MIWI and are involved in post-transcriptional regulation of target mRNAs and long non-coding RNAs (lncRNAs) in addition to retrotransposon silencing (Reuter *et al*, 2011; Beyret *et al*, 2012; Vourekas *et al*, 2012; Gou *et al*, 2014; Watanabe & Lin, 2014; Watanabe *et al*, 2015; Zhang *et al*, 2015). Although several reports indicate that the slicer activity of MIWI and pachytene piRNAs are essential for repressing transposons to maintain the genome integrity of male germ cells (Reuter *et al*, 2011; Zheng & Wang, 2012) and for preventing mRNA over-expression to sustain proper spermiogenesis (Gou *et al*, 2014; Zhang *et al*, 2015), little is known about MIWI-piRNA targeting of non-coding RNAs during meiosis.

In this study, we report that MIWI-piRNA complexes target pericentromere-derived major satellite transcripts and that such targeting leads to satellite RNA processing. Furthermore, we show that such satellite RNA processing is important for meiotic centromere cohesion and kinetochore assembly and works in parallel with a Dicer-dependent pathway to eliminate satellite transcripts, with both pathways required for proper meiotic chromosome segregation to prevent the transmission of aneuploidy to the next generation.

Results

Abrogation of MIWI causes chromosome mis-segregation

Our previous work demonstrated that *Miwi*-deficient mice display spermiogenic arrest at step 1 of round spermatid stage and an increase in apoptotic cells during spermatogenesis (Deng & Lin, 2002). In addition, it has been reported that the spindle assembly checkpoint is a key regulator of chromosome segregation in meiosis that prevents the production of aneuploid gametes that causes infertility and birth defects (Eaker *et al*, 2001; Sun & Kim, 2012; Gorbsky, 2015). It has also been shown that a consequence of checkpoint-detected error is apoptosis (Sinha Hikim & Swerdloff, 1999; Print & Loveland, 2000; Eaker *et al*, 2001). To investigate whether the early spermiogenic arrest and apoptosis of *Miwi* mutant spermatogenic cells reflect a function of the MIWI protein in meiotic checkpoint regulation, we examined the distribution of apoptotic cells in $Miwi^{-/-}$ testes using the TdT-mediated dUTP nick end labeling (TUNEL) assay. Consistent with previous observations, TUNEL labeling of testicular sections revealed significantly increased cell death in *Miwi* homozygotes ($Miwi^{-/-}$) as compared to *Miwi* heterozygotes ($Miwi^{+/-}$; Appendix Fig S1). Importantly, TUNEL-positive signals were detected in a sub-population of spermatocytes and round spermatids that express MIWI. These results support that *Miwi* is critical for the survival of meiotic and post-meiotic germ cells, including mid-to-late spermatocytes (mid-pachytene, diplotene, and diakinesis) and round spermatids. Notably, confocal images revealed that a proportion of TUNEL-positive staining in metaphase I stage presented a small punctate pattern that coincides with DAPI signal (Fig 1A, asterisk). This specific punctate pattern reflects that chromosomes are not properly aligned on the metaphase plate, and thus, MIWI might be required for metaphase plate alignment.

To further verify the role of MIWI in the formation of the metaphase plate, we compared the frequency of chromosome misalignment between *Miwi* heterozygotes and homozygotes. We performed immunofluorescence microscopy using antibodies against the phosphorylated form of histone H3-Ser10 to visualize condensed chromosomes at G2/M in spermatocytes (Cobb *et al*, 1999) and against α/β-tubulin to outline meiotic spindles. In contrast to *Miwi* heterozygotes, the metaphase I (MI) of *Miwi* homozygous spermatocytes showed a conspicuous increase in unaligned or misaligned chromosomes (*cf.* Fig 1B and C; quantified in D). This defect was accompanied by an increase in abnormal karyotype in metaphase II (MII) spermatocytes (Fig 1E–G), as characterized by significantly higher incidence of cells with at least one missing (< 20 chromosomes per cell) or extra (> 20 chromosomes per cell) chromosome, indicating a higher frequency of aneuploid haploid cells in *Miwi*-null mice. On the other hand, the occurrence of abnormal chromosome number in MI (Fig 1H–J) was not significantly different between *Miwi* heterozygotes and homozygotes, indicating that the aneuploidy haploid cells are likely caused by chromosome mis-segregation during meiosis I. Expectedly mitotic spermatogonia or somatic cells that do not express MIWI do not show an increase in the incidence of abnormal chromosomes in the *Miwi* mutant (Fig 1K–M). These results indicate that *Miwi* plays a role in the regulation of chromosome segregation during meiosis I to prevent abnormal segregation of chromosomes and aneuploidy.

Although an increase in cell death was detected at meiotic metaphases of *Miwi*-deficient meiotic cells (Fig 1A), the aneuploid secondary spermatocytes were still generated (Fig 1E–G). This implies that, during male meiosis, the spindle assembly checkpoint mechanism does not efficiently eliminate all germ cells with

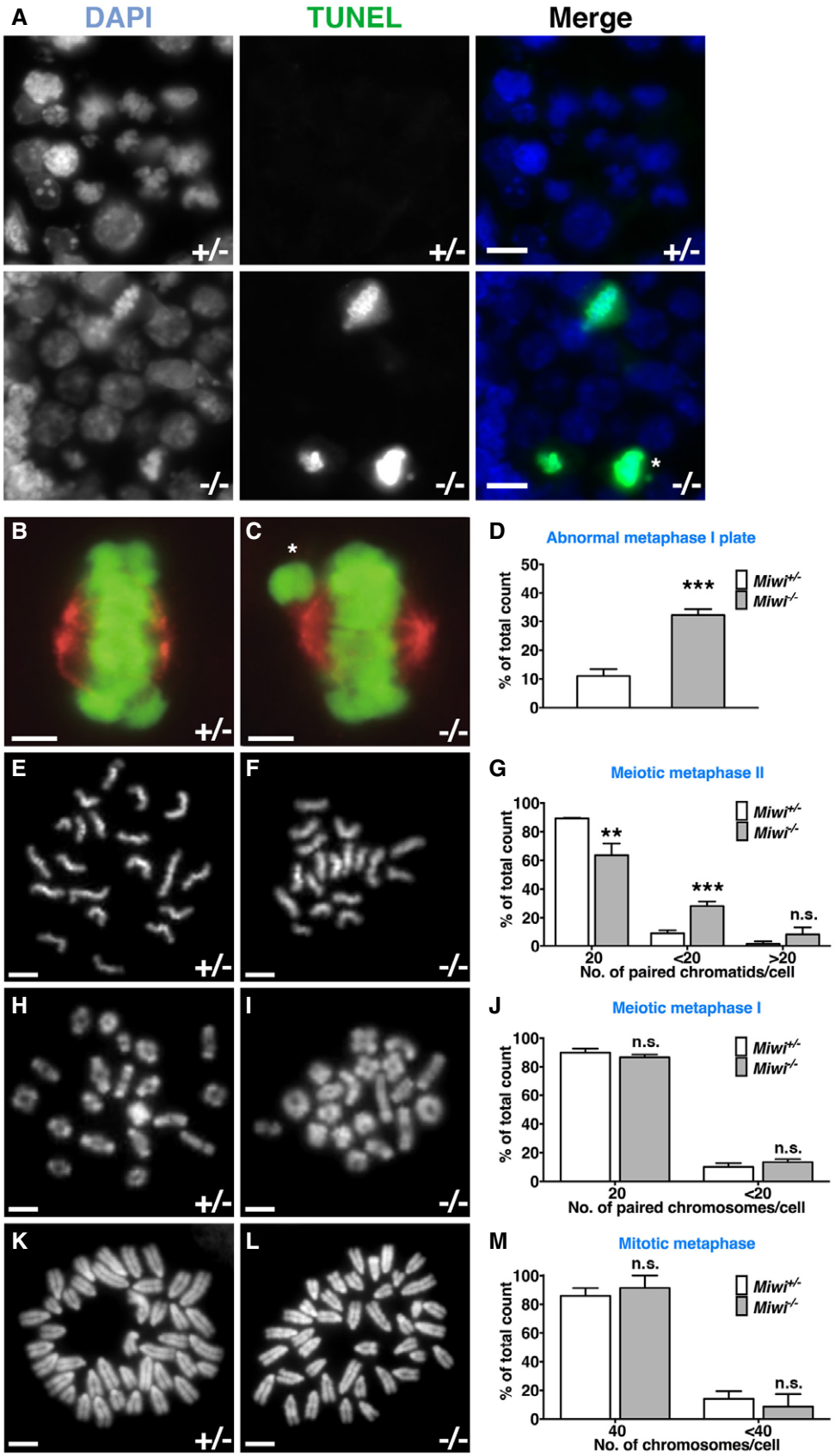
A
DAPI
TUNEL
Merge
+/-
-/-
B
C
D
Abnormal metaphase I plate
% of total count
Miwi+/-
Miwi-/-
***
E
F
G
Meiotic metaphase II
**
n.s.
20
<20
>20
No. of paired chromatids/cell
H
I
J
Meiotic metaphase I
No. of paired chromosomes/cell
K
L
M
Mitotic metaphase
40
<40
No. of chromosomes/cell

Figure 1.

Figure 1. Increased frequency of cell death and chromosome segregation defects in *Miwi*$^{-/-}$ spermatocytes.

A TUNEL assay comparing apoptotic cells in *Miwi*$^{+/-}$ and *Miwi*$^{-/-}$ testis during diakinesis. Blue, DAPI; Green, TUNEL labeling. Asterisk indicates TUNEL-positive stained cells in the meiotic metaphase stage. Scale bars, 10 μm.

B, C Meiotic metaphase I plate in FACS-sorted *Miwi* heterozygous (B) and knockout (C) spermatocytes. Green: phospho-histone H3; red: α/β-tubulin. Asterisk indicates misaligned chromosome. Scale bars, 10 μm.

D Frequency of abnormal arrangement in the meiotic metaphase I plate. White, *Miwi* heterozygous; Light gray, *Miwi* knockout. Three mice were used for each genotype, and total numbers of counted metaphase I plate in *Miwi* heterozygous and knockout are 113 and 181, respectively.

E, F Meiotic metaphase II spread preparations of *Miwi* heterozygous (E) and knockout (F) spermatocytes. Scale bars, 5 μm.

G Frequency of meiotic metaphase II (MII) cells with chromosomal abnormalities. Chromosome counts were defined as the number of paired sister chromatids per MII metaphase cell. The frequency was calculated as the number of cells with given pairs of sister chromatids (20, < 20, or > 20) divided by the total number of cells. Three mice were used for each genotype, and total numbers of counted MII cells in *Miwi* heterozygous and knockout are 204 and 302, respectively.

H, I Meiotic metaphase I spread preparations of *Miwi* heterozygous (H) and knockout (I) spermatocytes. Scale bars, 5 μm.

J Frequency of meiotic metaphase I (MI) cells with chromosomal abnormalities. Chromosome counts were defined as the number of paired homologous chromosomes per MI metaphase cells. The frequency was calculated in the same way as in (G), except for that the number of paired chromosomes was counted instead. Three mice were used for each genotype, and total numbers of counted MI cells in *Miwi* heterozygous and knockout are 265 and 358, respectively.

K, L Mitotic metaphase spread preparations of *Miwi* heterozygous (K) and knockout (L) testes. Scale bars, 5 μm.

M Frequency of mitotic metaphase cells with chromosomal abnormalities. Chromosome counts were defined as the number of chromosomes per mitotic metaphase cell. Three mice were used for each genotype, and total numbers of counted mitotic metaphase cells in *Miwi* heterozygous and knockout are 52 and 71, respectively.

Data Information: In (D), (G), (J), and (M), the results are presented as the mean ± SD of three independent experiments. The statistical test was assessed using two-tailed unpaired *t* test (**$P < 0.01$; ***$P < 0.001$; n.s., $P > 0.05$). +/−, *Miwi* heterozygous; −/−, *Miwi* knockout.
Source data are available online for this figure.

chromosomal abnormalities, which is in line with previous findings (Eaker *et al*, 2001). Consequently, this may escalate the occurrence of apoptosis in post-meiotic germ cells (Appendix Fig S1), due to genomic instability and developmental toxicity.

Loss of MIWI leads to over-expression of centromere and pericentromere non-coding RNAs

Because the known function of MIWI is in post-transcriptional regulation of mRNA, lncRNA, and transposon RNA (Deng & Lin, 2002; Reuter *et al*, 2011; Watanabe *et al*, 2015), we investigated whether MIWI regulates centromere- and pericentromere-encoded RNAs that are thought to be involved in chromosome segregation. DNA corresponding to the centromere and pericentromere consists of extensive arrays of short tandem repeats, termed minor and major satellites, respectively, that have long been thought to be transcriptionally inert. However, research in the past decade has unequivocally demonstrated the expression of centromere- and pericentromere-derived non-coding RNAs across different eukaryotic species (Chen *et al*, 2008; Eymery *et al*, 2009b) as well as their critical role in establishing centromeric identity and pericentromeric heterochromatin, in organizing kinetochore architecture, and in chromosome segregation (Gent & Dawe, 2012; Rosic *et al*, 2014; Caceres-Gutierrez & Herrera, 2017; Velazquez Camacho *et al*, 2017). To investigate whether MIWI could regulate the expression of repetitive satellite RNAs transcribed from centromeric and pericentromeric regions, we examined the expression levels of minor and major satellite transcripts in *Miwi* heterozygote, knockout, and slicer activity-deficient mutant spermatocytes. Northern blot and quantitative RT–PCR assays revealed an approximately 1.5- to 3-fold increase in the levels of RNAs transcribed from both orientations of major and minor satellite repeats in the *Miwi*-knockout and slicer activity-deficient spermatocytes as compared to *Miwi*$^{+/-}$ spermatocytes (Fig 2A and B; for verification of the sequence specificity and strand specificity of the Northern probes for satellite RNAs, see Materials and Methods and Appendix Fig S2).

To examine whether the observed over-expression of satellite RNAs in the mutant spermatocytes was actually due to a change in the composition and/or number of spermatocytes in the mutants, we prepared meiotic chromosome spreads to define each sub-stage of spermatocyte, using antibodies against synaptonemal complex proteins 1 and 3 (SCP1 and 3) that are components of the transverse and axial/lateral elements of the synaptonemal complex, respectively. At 21–24 days postpartum (dpp), there was no significant difference in either the composition or the number of different types of spermatogenic cells between *Miwi* knockout and heterozygote (Appendix Fig S3). These results indicate a role for MIWI in repressing the expression of centromere- and pericentromere-encoded RNAs that relies on its catalytic activity. Thus, MIWI appears to regulate the expression of repetitive satellite RNAs negatively.

Satellite RNA over-expression is the cause of chromosome segregation

To investigate the potential causal relationship between satellite RNA over-expression and chromosome mis-segregation, we over-expressed satellite RNAs in spermatocytes isolated from 20 dpp *Miwi*$^{+/-}$*;Stra8-Cre* testis and in co-culture with Sertoli cells and assessed the effect of the over-expression on meiosis (Tres & Kierszenbaum, 1983, 1999; Marh *et al*, 2003; Matsuda & Cepko, 2007). To achieve over-expression, we constructed major and minor satellite repeats that contain 8 and 14 repeat units, respectively, into a Cre-dependent expression vector (Matsuda & Cepko, 2007) containing the CAG promoter with a floxed stop cassette. Co-transfection of two plasmids expressing opposite strands of major or minor satellite RNA was performed after cells were plated for 6 h. 72-h after transfection, MIWI-expressing spermatocytes were FACS-sorted and harvested. The expression of satellite RNAs was confirmed by quantitative RT–PCR analyses (Fig 2C–G). Spermatocytes transfected with the empty vector were used as a negative control. We found that spermatocytes over-expressing both strands of either major or minor satellite RNAs showed a significant increase in frequency of chromosome misalignment as observed in *Miwi*-knockout

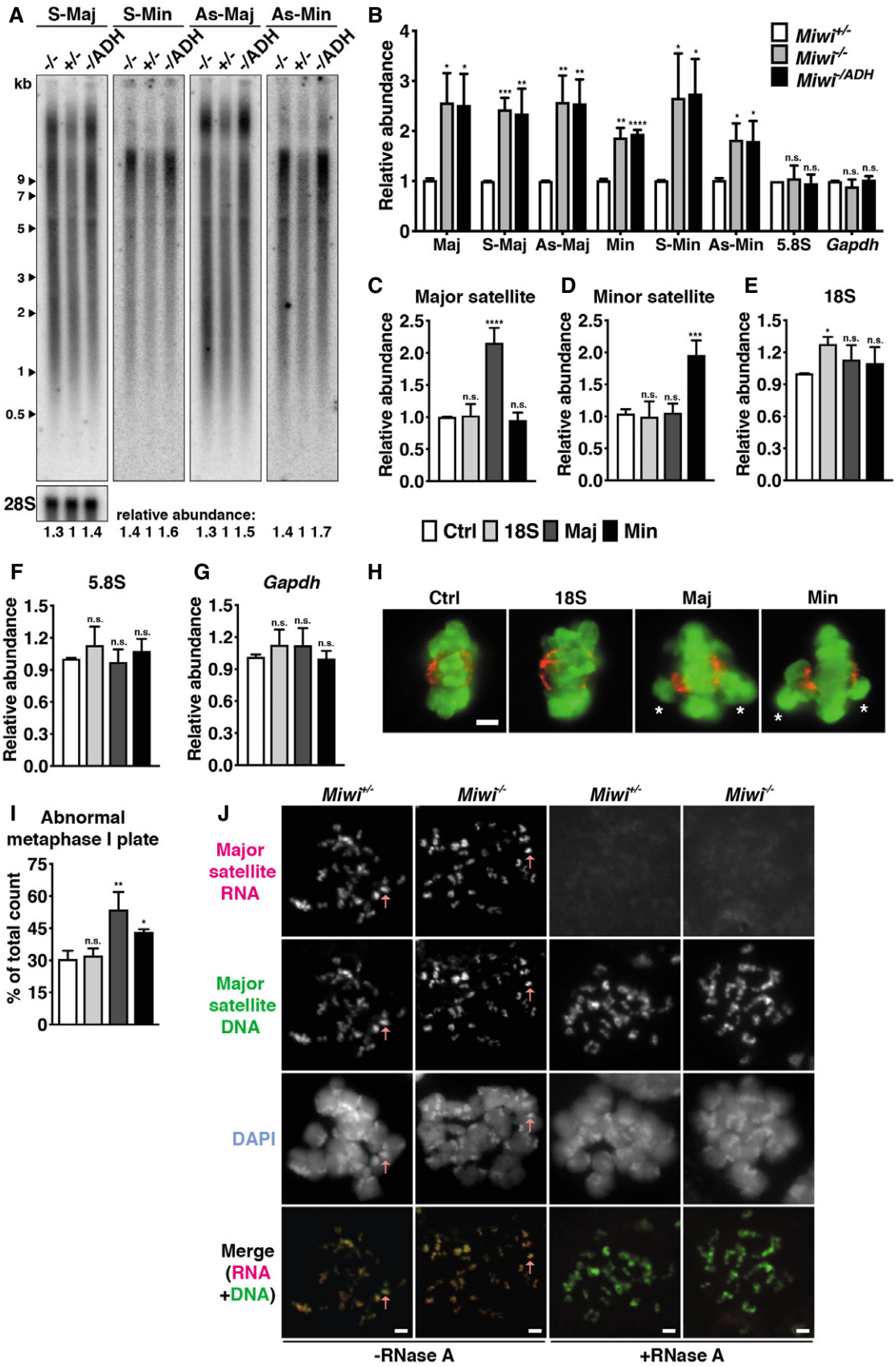
A
S-Maj
S-Min
As-Maj
As-Min
-/-
+/-
-/ADH
kb
9
7
5
3
2
1
0.5
28S
relative abundance:
1.3 1 1.4
1.4 1 1.6
1.3 1 1.5
1.4 1 1.7
B
Miwi+/-
Miwi-/-
Miwi-/ADH
Relative abundance
Maj
S-Maj
As-Maj
Min
S-Min
As-Min
5.8S
Gapdh
C
Major satellite
D
Minor satellite
E
18S
Ctrl
18S
Maj
Min
F
5.8S
G
Gapdh
H
Ctrl
18S
Maj
Min
I
Abnormal metaphase I plate
% of total count
J
Miwi+/-
Miwi-/-
Miwi+/-
Miwi-/-
Major satellite RNA
Major satellite DNA
DAPI
Merge (RNA +DNA)
-RNase A
+RNase A

Figure 2.

Figure 2. Over-expression of satellite transcripts in *Miwi*-knockout and *Miwi* slicer-deficient spermatocytes causes chromosome mis-segregation during meiosis.

A Equal amounts of total RNA isolated from *Miwi*-knockout (−/−), heterozygote (+/−), and slicer activity-deficient mutant (−/ADH) spermatocytes were resolved on a 1% agarose gel. The gel was subjected to Northern blot analysis using probes specific for the sense (S) and antisense (As) strands of major (Maj) and minor (Min) satellite RNA transcripts. The blot was re-hybridized with a 28S-complementary probe to demonstrate equal loading (bottom on the left). The relative abundance was quantified using ImageJ software, normalized to the 28S signal from the blot.

B 100 ng of total RNA was isolated from *Miwi* heterozygous (+/−), knockout (−/−), and slicer activity-deficient mutant (−/ADH) spermatocytes and was subjected to qRT–PCR with primers specific to major satellite RNA, minor satellite RNA, 5S, 5.8S, and *Gapdh*. Data were normalized to 5S rRNA. 5.8S rRNA and *Gapdh* were used as negative controls.

C–G Sertoli-spermatogenic cell co-cultures were transfected with vectors ectopically expressing both strands of major satellite RNA (Maj, dark gray bar), both strands of minor satellite RNA (Min, black bar), full-length 18S (18S, light gray bar), or empty vector (Ctrl, white bar). Total RNA isolated from equal numbers of FACS-sorted MIWI-expressing spermatocytes were subjected to qRT–PCR with primers specific to major satellite RNA (C), minor satellite RNA (D), 18S (E), 5.8S (F), and *Gapdh* (G). Data presented were normalized to 5S rRNA. 5.8S rRNA (F) and *Gapdh* (G) were used as negative controls.

H Immunofluorescence images of Meiotic metaphase I plate in Sertoli-spermatogenic cell co-cultures. Shown were spermatocytes over-expressing both strands of major satellite RNA (Maj), both strands of minor satellite RNA (Min), full-length 18S (18S), or empty vector (Ctrl). Green: phospho-histone H3; red: α/β-tubulin. Asterisk indicates misaligned chromosome. Scale bar, 5 μm.

I Frequency of mis-arrangement of the meiotic metaphase I plate in Sertoli-spermatogenic cell co-cultures using *Miwi*$^{+/-}$;*Stra8-Cre* testes. Spermatocytes transfected with vectors expressing both strands of major satellite RNA (Maj, dark gray), both strands of minor satellite RNA (Min, black), full-length 18S (18S, light gray), or empty vector (Ctrl, white). n = 3 cultures for each group. The total numbers of counted meiotic metaphase plate in Ctrl, 18S, Maj, and Min were 153, 144, 130, and 141, respectively.

J Combined RNA-DNA FISH analysis of major satellite transcripts and DNA regions in *Miwi* heterozygote (*Miwi*$^{+/-}$) and knockout (*Miwi*$^{-/-}$) diakinesis spermatocytes. Sense major satellite RNA transcripts were first detected using an antisense probe (red signal), and then, the major satellite DNA region was further detected using a sense probe (green signal). For RNase A treatment, the slides were incubated with (+RNase A) or without (-RNase A) 100 μg/ml RNase A for 1 h before adding antisense probe. Nuclear DNA was stained by DAPI (blue). Arrows indicate the same pericentric heterochromatin in each channel per cell. Scale bars represent 2 μm.

Data information: The results represent the mean ± SD of three independent experiments. The statistical test was assessed using two-tailed unpaired *t* test. *$P < 0.05$; **$P < 0.01$; ***$P < 0.001$; ****$P < 0.0001$; n.s., $P > 0.05$. Maj: total major satellite RNA; S-Maj: sense major satellite RNA; As-Maj: antisense major satellite RNA; Min: total minor satellite RNA; S-Min: sense minor satellite RNA; As-Min: antisense minor satellite RNA.
Source data are available online for this figure.

spermatocyte (Fig 2H and I), indicating that the over-expression of either major or minor satellite RNAs triggers chromosome misalignment in meiosis I. As a second negative control, the spermatocytes over-expressing the 18S rRNA did not affect satellite RNA expression or chromosome alignment (Fig 2E and I).

We then investigated whether reducing satellite RNA expression in spermatocytes could decrease the frequency of chromosome misalignment. To reduce satellite RNA expression, we expressed satellite RNA-complementary short hairpin RNA (shRNA) in spermatocyte–Sertoli co-cultures from 20 dpp *Miwi*$^{-/-}$;*Stra8-Cre* testes. The expression of strand- and satellite RNA-specific shRNA oligos was achieved by inserting the shRNA-encoding DNA sequence into a Cre-dependent plasmid vector, pSico, that contains a U6 promoter with a flox-flanked CMV-driven reporter-stop cassette (Ventura *et al*, 2004; we replaced EGFP with mCherry for our purpose). After Cre-mediated recombination, the cassette was excised, allowing U6-driven expression of shRNA expression. The empty vector and vector carrying a scrambled shRNA were used as negative controls. The extent of knockdown was quantified by RT–qPCR (Appendix Fig S4A–D). The spermatocytes with the knockdown of both strands of major or minor satellite RNAs showed lower frequencies of chromosome misalignment as compared to the cells expressing the empty vector or control shRNA (Appendix Fig S4E). This indicates that a lower-than-wild-type level of satellite RNAs actually improves chromosome alignment in meiosis I. Unexpectedly, spermatocytes expressing major satellite-specific shRNAs showed decreased minor satellite RNA expression, but spermatocytes expressing control shRNAs show no effect on satellite RNA expression or chromosome alignment (Appendix Fig S4). These observations imply that the expression of minor satellite RNA somehow depends on major satellite RNA.

Loss of MIWI leads to mis-localization of kinetochore proteins in Meiosis I

We then investigated how satellite RNA over-expression causes chromosome mis-segregation. Previous reports have demonstrated that, in mitosis, nascent centromeric transcripts are important for recruiting the remodeling complex required to modify centromere chromatin (Gent & Dawe, 2012). However, the accumulation of satellite transcripts can cause mis-localization of centromere-associated proteins, defects in kinetochore assembly, and chromosome segregation, resulting in aneuploidy (Bouzinba-Segard *et al*, 2006; Hsieh *et al*, 2011; Huang *et al*, 2015; Grenfell *et al*, 2016). In addition, an increase in major satellite RNA causes chromosome instability and over-expression of centromeric cohesin in the cleavage-stage embryo (De La Fuente *et al*, 2015). Indeed, the over-expression of these transcripts in mouse and human cancers is considered to impair genome stability and facilitate cell transformation (Eymery *et al*, 2009b; Ting *et al*, 2011; Kishikawa *et al*, 2016). Therefore, we investigated whether the accumulation of the satellite transcripts in *Miwi*-deficient spermatocytes (Fig 2A and B) affects the assembly of centromere-associated proteins in the centromere region. We first examined the localization of the satellite transcripts by combined RNA and DNA fluorescence *in situ* hybridization (FISH) analysis. The signals for major satellite transcripts and satellite DNA were validated by RNase A sensitivity resistance, respectively. This analysis revealed that *Miwi* heterozygote and knockout spermatocytes show similar localization of major satellite transcripts that overlap with hourglass-shaped satellite DNA organization at each chromosome (Fig 2J). Thus, MIWI deficiency does not visibly alter the centromeric localization of satellite transcripts in spermatocytes.

To examine whether the overly abundant satellite transcripts at the centromere affects the architecture of sister kinetochores in MI spermatocytes, we performed immunofluorescence analysis using CREST antisera to mark the inner plate of the kinetochore, followed by DNA FISH to label major satellite repeats. In either *Miwi* heterozygote or knockout spermatocytes, all the CREST foci were flanked by hourglass-shaped satellite DNA signals except for the foci at the Y chromosome that lacks the major satellite sequence at the pericentromere (Fig 3A). This indicates that MIWI is dispensable for the loading of centromere proteins to chromosomes.

We then examined whether sister kinetochores are properly aligned. Normally, a pair of sister kinetochores form a single coherent unit to provide a shared microtubule-binding surface for the co-segregation of sister chromatids in MI (Li & Dawe, 2009; Sarangapani *et al*, 2014). Such as coherent unit is reflected by CREST staining as a single focus. However, *Miwi*-knockout spermatocytes often contain more than 40 CREST foci—the normal number of paired sister kinetochores in a wild-type MI spermatocyte (Fig 3A–C). This raised the possibility that two individual kinetochores in a sister kinetochore pair are separated from each other, thus appearing as two units. To verify this possibility, we examined each pair of sister kinetochores (Fig 3B) that was flanked by the same satellite DNA signal in *Miwi* heterozygote, knockout, and slicer-deficient spermatocytes. We classified sister kinetochore pairs as "overlapping" (a single spot in which two sister kinetochores overlap by > 100% of their individual radii), "adjacent" (two sister kinetochores overlap by < 100% of their individual radii), or "separated" (two sister kinetochores which do not overlap at all; Figs 3A and B, and EV1A). Although the majority of sister kinetochore pairs in all genotypes were overlapping pairs, the percentage of overlapping pairs in both *Miwi* homozygotes and slicer-deficient mutants was significantly lower than in *Miwi* heterozygotes (90.1%, 77.8%, and 79.8% in $Miwi^{+/-}$, $Miwi^{-/-}$, and $Miwi^{-/ADH}$, respectively; Fig 3C). Correspondingly, the percentage of adjacent pairs in *Miwi* homozygotes and slicer-deficient spermatocytes was significantly higher than in *Miwi* heterozygotes (9.7%, 21.7%, and 19.9% in $Miwi^{+/-}$, $Miwi^{-/-}$, and $Miwi^{-/ADH}$, respectively). Similarly, higher frequencies of separated pairs were seen in the mutants, even though the difference was not statistically significant due to the rare occurrence of this type of defect (0.2%, 0.5%, and 0.3% in $Miwi^{+/-}$, $Miwi^{-/-}$, and $Miwi^{-/ADH}$, respectively). These results indicate that MIWI and its slicer activity are important for the inner plate of a sister kinetochore pair to organize as a single coherent unit in MI.

The kinetochore is a proteinaceous multi-subunit assembly, consisting of an inner plate, an outer plate, and a fibrous corona (Musacchio & Desai, 2017) (Fig 3B). Although non-overlapping inner plates in the *Miwi* mutants may cause separated outer plates between sister chromatids, it is possible that outer plates still form coherently to ensure sister chromatid co-segregation, as observed in maize MI (Li & Dawe, 2009). To examine the organization of kinetochore outer plates in *Miwi* heterozygote, knockout, and slicer-deficient mutant spermatocytes, we performed combined immunofluorescence and DNA FISH using CREST antisera to mark the inner plate and anti-BubR1 antibodies to mark the outer plate, followed by DNA FISH to label major satellite repeats. This allowed us to further classify sister kinetochore pairs by considering the configuration of not only inner but also outer plates (Figs 3D–E and EV1B), both of which were classified as "overlapping", "adjacent", or "separated", as defined above. We then designated "O" for the overlapping type and "S" for combined adjacent and separated types that reflect pairing defects. In all genotypes, the majority of kinetochore pairs were overlapping pairs with regard to both inner and outer plates, herein designated as

Figure 3. *Miwi*-null and *Miwi* slicer-deficient spermatocytes show a reduced number of coherent sister kinetochores in meiosis I.

A Combined immunofluorescence and DNA FISH analysis of the kinetochore inner plate/centromere formation in *Miwi* heterozygous ($Miwi^{+/-}$) and knockout ($Miwi^{-/-}$) spermatocytes at diakinesis/metaphase I. For slicer activity-deficient mutant spermatocytes ($Miwi^{-/ADH}$), the images are presented in Fig EV1A. Chromosomes were stained with anti-centromere protein antibody (CREST, purple signal), indicating the kinetochore inner plate/centromere. Major satellite DNA regions were detected using an antisense probe (red signal) which revealed the specific localization of pericentromeres in chromosomes. Nuclear DNA was stained by DAPI (blue). Scale bars represent 2 μm.

B Left panel: illustration of kinetochore configurations in meiotic metaphase I. The kinetochores of sister chromatids cohere to form a single microtubule-binding interface. The inner–outer kinetochore axis connects the pericentric chromatin to the spindle microtubule. CREST (centromere protein) and BUBR1 (budding uninhibited by benzimidazole-related 1) served as markers for the inner and outer regions of the kinetochore, respectively. A major satellite DNA (Maj sat DNA) probe was used to detect the pericentric chromatin. Right panel: categories of inner kinetochore configurations from A. Right panels: Inner kinetochore configurations in MI were classified as overlapping (two sister kinetochores which overlap by more than their individual radii, also see yellow arrow in A), adjacent (two sister kinetochores which overlap by less than 100% of their individual radii, also see magenta arrow in A), or separated (two sister kinetochores without overlapping, also see light blue arrow in A) kinetochores. The scale bar represents 1 μm.

C Population of overlapping, adjacent, and separated inner kinetochores shown in B. The results represent the mean ± SD of three independent experiments. $n = 3$ mice for each genotype. The total numbers of counted cells in $Miwi^{+/-}$, $Miwi^{-/-}$, and $Miwi^{-/ADH}$ spermatocytes were 88, 118, and 125, respectively. The total numbers of counted sister kinetochore pairs in $Miwi^{+/-}$, $Miwi^{-/-}$, and $Miwi^{-/ADH}$ spermatocytes were 3,520, 4,720, and 5,000, respectively.

D Combined immunofluorescence and DNA FISH analysis of kinetochore inner and outer plate formation in *Miwi* heterozygous ($Miwi^{+/-}$) and knockout ($Miwi^{-/-}$) at diakinesis/metaphase I. For slicer activity-deficient mutant spermatocytes ($Miwi^{-/ADH}$), the images are presented in Fig EV1B. Chromosomes were stained with anti-BUBR1 (green) and anti-centromere-protein (CREST, purple) antibodies to mark the kinetochore outer and inner plate, respectively. In addition, major satellite DNA regions were further detected using an antisense probe (red signal). Nuclear DNA was stained by DAPI (blue). O-O kinetochore pairs: yellow arrow; S-S, magenta arrow; O-S, light blue arrow; and S-O, light green arrow. Scale bars represent 2 μm.

E Magnified images of categories of sister kinetochore configurations from D. One arrow indicates overlapping pair. Double arrows indicate split pair. The scale bar represents 1 μm.

F Population of the sister kinetochores shown in E. $n = 3$ mice for each genotype. The total numbers of counted cells in $Miwi^{+/-}$, $Miwi^{-/-}$, and $Miwi^{-/ADH}$ spermatocytes were 93, 89, and 81, respectively. The total numbers of counted sister kinetochore pairs in $Miwi^{+/-}$, $Miwi^{-/-}$, and $Miwi^{-/ADH}$ spermatocytes were 3,720, 3,560, and 3,240, respectively.

Data information: Data represent the mean ± SD of three independent experiments. The statistical test was assessed using one-way ANOVA test (**$P < 0.01$; ***$P < 0.001$).
Source data are available online for this figure.

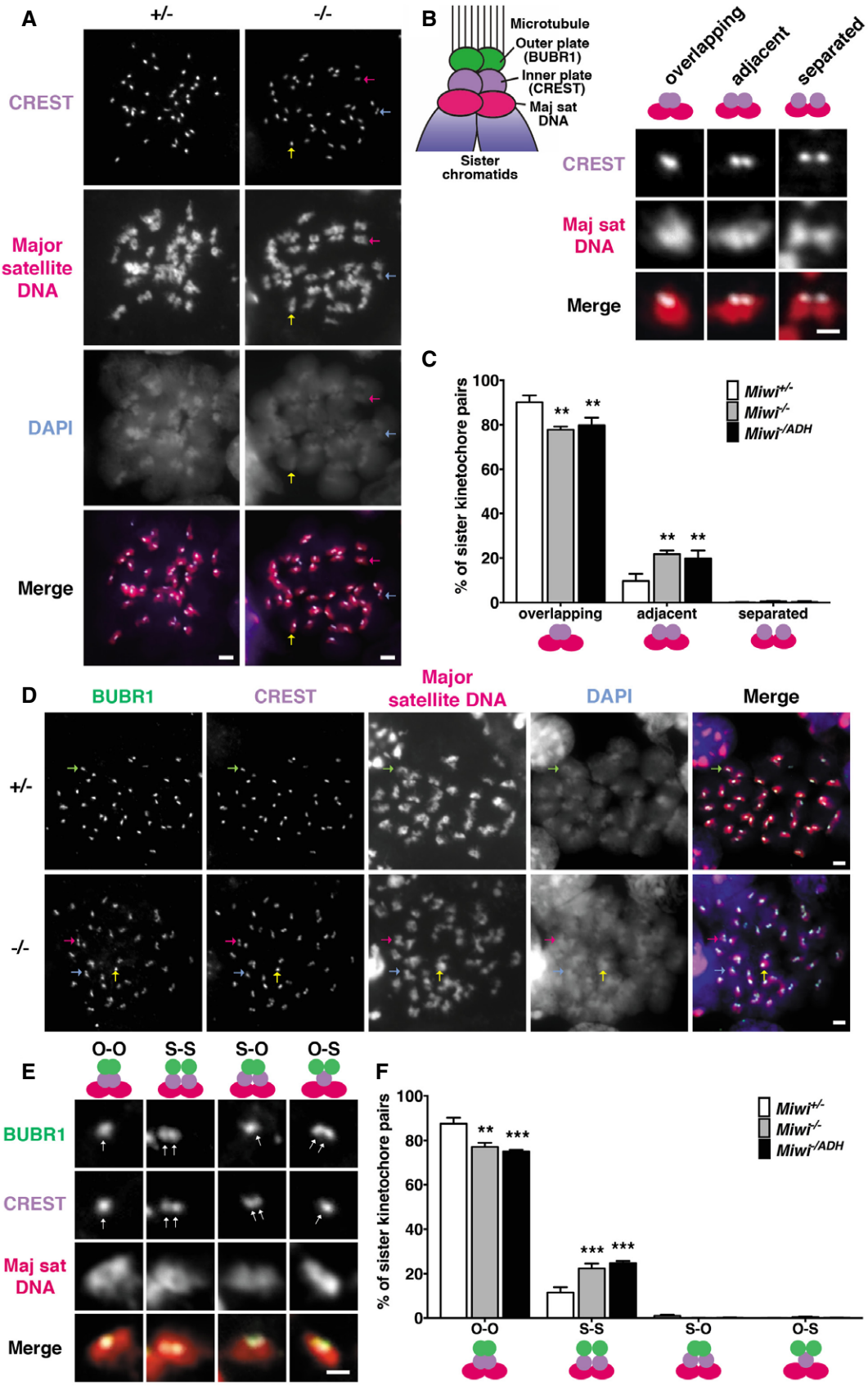

Figure 3.

"O-O" for "double overlapping" pairs (87.6%, 77.1%, and 75% in $Miwi^{+/-}$, $Miwi^{-/-}$, and $Miwi^{-/ADH}$, respectively). However, in both *Miwi* homozygotes and slicer-deficient mutants, the percentage of O-O pairs per spermatocytes was significantly lower than that of *Miwi* heterozygotes, yet the percentage of kinetochore pairs with both inner and outer plate adjacent or separated ("S-S") was significantly higher (11.4%, 22.4%, and 24.7% in $Miwi^{+/-}$, $Miwi^{-/-}$, and $Miwi^{-/ADH}$, respectively; Fig 3F).

To verify the defects in kinetochore organization as revealed by using CREST and BurbR1 as markers, we further used anti-CENP-A antibodies to mark the inner plate and anti-HEC1 antibodies to mark the outer plate, followed by DNA FISH to label major satellite repeats. The CENP-A and HEC1 loci co-localize with CREST and BUBR1, respectively (Appendix Fig S5A and B), and the frequencies of O-O and S-S pairs in *Miwi* heterozygote and knockout spermatocytes as marked by CENP-A and HEC1 were very similar to those as marked by CREST and BUBR1 (O-O pair: 86.8% in $Miwi^{+/-}$and 72.7% in $Miwi^{-/-}$; S-S pair: 12.7% in $Miwi^{+/-}$ and 26.6% in $Miwi^{-/-}$; Appendix Fig S5C–E). These results indicate that MIWI and its slicer activity promote the formation of a shared microtubule-binding face between a sister kinetochore pair in male MI. Moreover, these results (Figs 1G, 3F and Appendix Fig S5E) correlate the loss of kinetochore coherence with the high probability of chromosome mis-segregation and aneuploidy, similar to previous findings in aged human and mouse oocytes (Shomper *et al*, 2014; Patel *et al*, 2015; Zielinska *et al*, 2015).

Interestingly, in spermatocytes of all three genotypes, kinetochore pairs with adjacent or separated inner plates but overlapping outer plates ("S-O") and vice versa ("O-S") were extremely rare (Fig 3E and F). This reflects that the organization of outer kinetochores between sister chromatids might be largely dictated by that of inner kinetochores, as in human oocyte MI (Patel *et al*, 2015). Overall, results in this section indicate that MIWI has a critical role in the coherence of sister kinetochores during male MI, which is required for sister chromatids co-segregation.

MIWI has no effect on sister chromatid cohesion

To investigate whether MIWI deficiency also affects chromosome alignment and cohesion of the two sister kinetochore pairs at meiosis I, we first conducted meiotic chromosome spread assay of $Miwi^{+/-}$ and $Miwi^{-/-}$ prophase I spermatocytes using antibodies against REC8 to recognize the meiotic-specific cohesion subunit, SCP3 to label the axial (a.k.a. lateral) element of the synaptonemal complex, and CREST to mark the centromere. At pachytene and diplotene stages, $Miwi^{+/-}$ and $Miwi^{-/-}$ spermatocytes show similar dotty REC8 signals along the entire length of the sister chromatids, indicating that MIWI has no effect on the proper alignment of sister chromatids in meiotic prophase I. At metaphase I stage, the intensity of the REC8 signal in both $Miwi^{+/-}$ and $Miwi^{-/-}$ spermatocytes declines as meiosis proceeded but a significant amount of REC8 signal was still observed along the chromosome axes at which the homologous chromosomes were overlapped and at pericentromere regions (Appendix Fig S6A and B), consistent with previous findings (Lee *et al*, 2003; Watanabe, 2004).

To verify the normalcy of kinetochore cohesion in the mutant as indicated by the REC8 signal, we examined the expression and localization of *Shugoshin1* (SGO1), a pericentromeric protein implicated in protecting pericentromeric REC8 from degradation and in cohesiveness of sister chromatids during meiosis I (Clift & Marston, 2011). In *Miwi* heterozygous knockout mice, the SGO1 signal was observed at pericentromeric heterochromatin region in each chromosome (Appendix Fig S6C), implying that MIWI deficiency does not affect the proper conjunction of sister chromatid cohesions, consistent with our earlier observation (Fig 1H and I), in which we did not detect the severe cohesion defects within meiotic chromosome spreads. These results indicate that MIWI has no obvious effect on the establishment and progression of sister chromatid cohesion during meiosis I.

MIWI has no effect on DNA methylation or transcription in centromeric and pericentromeric regions

Although MIWI is a cytoplasmic protein involved in post-transcriptional regulation, it is possible that MIWI indirectly affects the transcription of satellite RNAs by regulating factors that are involved in epigenetic or transcriptional machineries. To test this possibility, we first compared the DNA methylation levels of satellite tandem repeats between *Miwi* heterozygote, knockout, and slicer activity-deficient spermatocytes. Equivalent amounts of DNA from spermatocytes of the three genotypes were digested either with the methylation-sensitive enzyme HpaII, or its methylation-insensitive isoschizomer MspI, and then subjected to Southern blot analysis. In all three genotypes, DNA from the centromeric region, the pericentromeric region, LINE1, and the housekeeping gene *Gapdh* had the similar levels of HpaII-digestion (Fig EV2A), reflecting that abolishing MIWI or its slicer activity does not significantly alter the methylation state of satellite repeat DNA or other tested genomic sequences, consistent with previous observations on LINE1 (Reuter *et al*, 2011).

To definitely examine whether MIWI affects the transcription of major and minor satellite repeat regions, we conducted the nuclear run-on assay. Intact nuclei from *Miwi* heterozygote, knockout, and slicer-deficient spermatocytes were pulsed with biotin-16-UTP. Newly synthesized biotin-labeled RNA was isolated by streptavidin beads and were then subjected to RT–qPCR assay to measure the relative abundance of newly synthesized major and minor satellite repeat transcripts as normalized against newly labeled U5 snRNA. The relative abundance of total major and minor satellite repeat transcripts in total RNA from corresponding genotypes against that of total U5 snRNA was also measured for comparison. We did not detect a significant difference in the abundance of newly transcribed major and minor satellite transcripts among the three genotypes. In contrast, the total level of these transcripts in *Miwi*-knockout or catalytic mutant spermatocytes was increased by threefold to fourfold, as expected (Fig EV2B). These results indicate that MIWI regulates the expression of satellite RNAs not at the transcriptional level, but rather at the post-transcriptional level. Finally, neither total nor nascent 5.8S rRNA, which is transcribed from repetitive ribosomal DNA, was changed in the mutants (Fig EV2B). These observations indicate that MIWI has a specific effect on the steady-state levels of major and minor satellite transcripts.

MIWI binds to pericentromere-encoded RNA transcripts

Although MIWI is enriched in the intermitochondrial cement and the nuage in the cytoplasm of spermatocytes as well as in the

chromatoid body in spermatids (Meikar *et al*, 2011; Nguyen-Chi & Morello, 2011; Tanaka *et al*, 2011), it can enter the nucleus at the end of diakinesis when these cytoplasmic structures and the nuclear envelope disperse (Kotaja *et al*, 2006). Hence, MIWI may enter the nucleus to process the satellite transcripts during prometaphase I when kinetochore proteins are loaded to the centromere (Parra *et al*, 2009). To demonstrate possible MIWI association with the satellite RNAs, we first performed RNA pull-down assays using *in vitro* transcribed, biotinylated RNA probes corresponding to approximately one unit of the major and minor satellite repeats (Fig 4A). To assess possible strand-specific binding, probes for major and minor satellite repeats were strand-specific. For both major and minor satellite sequences, we refer T- and A-rich transcript as "sense" and "antisense" transcript, respectively, following the previous nomenclature (Falconer *et al*, 2010; Saksouk *et al*, 2015). The probes were then mixed with 21–24 dpp testicular extracts, followed by adding streptavidin-coated beads to pull down the probes. The resulting precipitates were analyzed by Western blot analysis, which showed that wild-type and catalytic mutant MIWI were efficiently co-precipitated with both sense and antisense strands of the major and minor satellite RNAs (Fig 4B, left panel). This indicates that MIWI binds to satellite RNAs independently of its slicer activity. Notably, MIWI association with sense and antisense strands of satellite RNAs was not significantly affected in *Mov10l1* germline knockout mice that are defective in pachytene piRNA biogenesis (Frost *et al*, 2010; Watanabe *et al*, 2015). This reflects that either MIWI binding to the satellite RNAs is either piRNA-independent or *Mov10l1* germline knockout mice still contain piRNAs targeting the satellite transcripts. Under the same experimental conditions, no binding was observed between the GAPDH protein or the Pumillio 1 RNA-binding protein and satellite RNAs (Fig 4B, right panel and Appendix Fig S7), or between MIWI and partial sequences of 18S rRNA (Fig 4B) or *Gapdhs* mRNA that were the similar lengths as satellite RNAs (Appendix Fig S7). These results indicate that MIWI associates with satellite RNAs with some specificity.

Intriguingly, MILI did not bind to satellite RNAs in the presence of MIWI but in the absence of MIWI or its slicer activity (Fig 4B, middle panel). This implies that satellite RNAs prefer to associate with MIWI but can bind to MILI when MIWI is absent. Finally, similar to MIIWI, MILI binds to satellite RNA in *Mov10l1* germline knockout mice (Fig 4B, middle panel and Appendix Fig S7), indicating that MILI binding to satellite RNA is either piRNA-independent or *Mov10l1* germline knockout mice still contain piRNAs targeting the satellite transcripts.

MIWI cleaves pericentromere-encoded RNA transcripts

To characterize the function of MIWI association with satellite RNAs, we performed RNA cleavage assay using *in vitro* transcribed, 5′-^{32}P-labeled minor and major satellite RNAs corresponding to approximately one or two units of the major and minor satellite repeats as substrates (Fig 4A). The substrates were incubated with nuclear extracts that contained the perinuclear nuage enriched with MIWI (Appendix Fig S8). Denaturing acrylamide gel electrophoresis revealed that the reaction mix containing MIWI and one repeat unit of the *in vitro* transcribed sense major satellite RNAs yielded a ~120 nt 5′ cleavage product (Fig 4C, left panel). This product was not detected when MIWI was either absent or was replaced by its slicer mutant. The reaction mix containing MIWI and two repeat units of sense major satellite RNAs also yielded a ~120 nt 5′ cleavage product (Fig 4C, left). These data indicate that MIWI cleaves a specific site on each repeat unit of the sense major satellite transcripts and that this cleavage relies on its slicer activity. This conclusion is also supported by Northern blot analysis that revealed an accumulation of satellite RNAs in MIWI catalytic mutants (Fig 2A). However, antisense major satellite RNAs and both strands of minor satellite RNAs were not cleaved (Fig 4C, middle panel).

Figure 4. MIWI binds to and processes major satellite RNAs.

A Schematic diagram showing organization of mouse major and minor satellite repeats. Major and minor satellite sequences comprise six megabases of a 234-bp repeats and six hundred kilobases of a 120-bp repeats, respectively. The terms "sense (S)" and "antisense (As)" refer to T- and A-rich transcripts, respectively. The length of major and minor satellite sequences used to perform *in vitro* transcription is indicated.

B RNA pull-down assay using biotinylated major and minor satellite RNA transcripts and whole-cell extracts from *Miwi* heterozygous (*Miwi*$^{+/-}$), knockout (*Miwi*$^{-/-}$), slicer activity-deficient mutant (*Miwi*$^{-/ADH}$), and *Mov10l1* germline knockout (*Mov10l1*$^{f/-}$;*Stra8-Cre*) testes. *Mov10l1*$^{f/-}$;*Stra8-Cre* mice represent a pachytene piRNA-deficient condition. Approximately one repeat of *in vitro* transcribed major and minor satellite RNAs corresponding to the sequences in A was used as baits. Precipitated proteins were visualized by Western blotting using antibodies against the indicated proteins (MIWI and MILI). The input equals 1/10 to 1/80 of the protein lysate used in the pull-down. Transcripts corresponding to 300 nt and 162 nt of the 18S rRNA sequence served as controls for the antisense (As) and sense (S) sequence of major and minor satellite transcripts, respectively. The blot was re-probed with anti-GAPDH antibody serving as a negative control.

C *In vitro* RNA processing assay with nuage–nuclear fraction from testicular lysates of *Miwi*-knockout (−/−), heterozygous (+/−), and slicer activity-deficient (−/ADH) mutants, and 5′-end radioactively labeled RNA targets corresponding to approximately one and two repeats of major and minor satellite sequences (see panel A for details). Transcripts corresponding to 162, 300, and 542 nt of the 18S rRNA sequence served as controls. Arrow indicates the cleavage products of *in vitro* transcribed sense major satellite RNAs after reactions.

D *In vitro* RNA processing assay with nuage–nuclear fraction from *Mov10l1* heterozygous (*Mov10l1*$^{f/+}$;*Stra8-Cre*) and *Mov10l1* germline knockout (*Mov10l1*$^{f/-}$;*Stra8-Cre*) testis lysates, and 5′-end radioactively labeled RNA targets corresponding to approximately one and two repeats of sense and antisense major satellite sequences. *Mov10l1*$^{f/-}$;*Stra8-Cre* mice represent a pachytene piRNA-deficient condition. The arrow indicates the cleavage product of the *in vitro* transcribed sense major satellite RNA.

E Major satellite RNA with respective piRNA target sequences. piR major-a and major-b target the sense strand of major satellite transcripts at their cleavage sites. The MIWI slicer activity results in 125- and 119-nt cleavage products.

F RNA immunoprecipitation was performed using anti-MIWI antibody. RNA was extracted from anti-MIWI immunoprecipitates and subjected to Northern blot analysis using probes specific for potential piRNAs (piR major-a and major-b), as indicated in panel E. 20% of input RNA from each group was used as the control. The blot was re-hybridized with piR-A and piR-E complementary probes to demonstrate the efficiency of the RNA-IP. A miR-16 complementary probe served as a negative control.

Source data are available online for this figure.

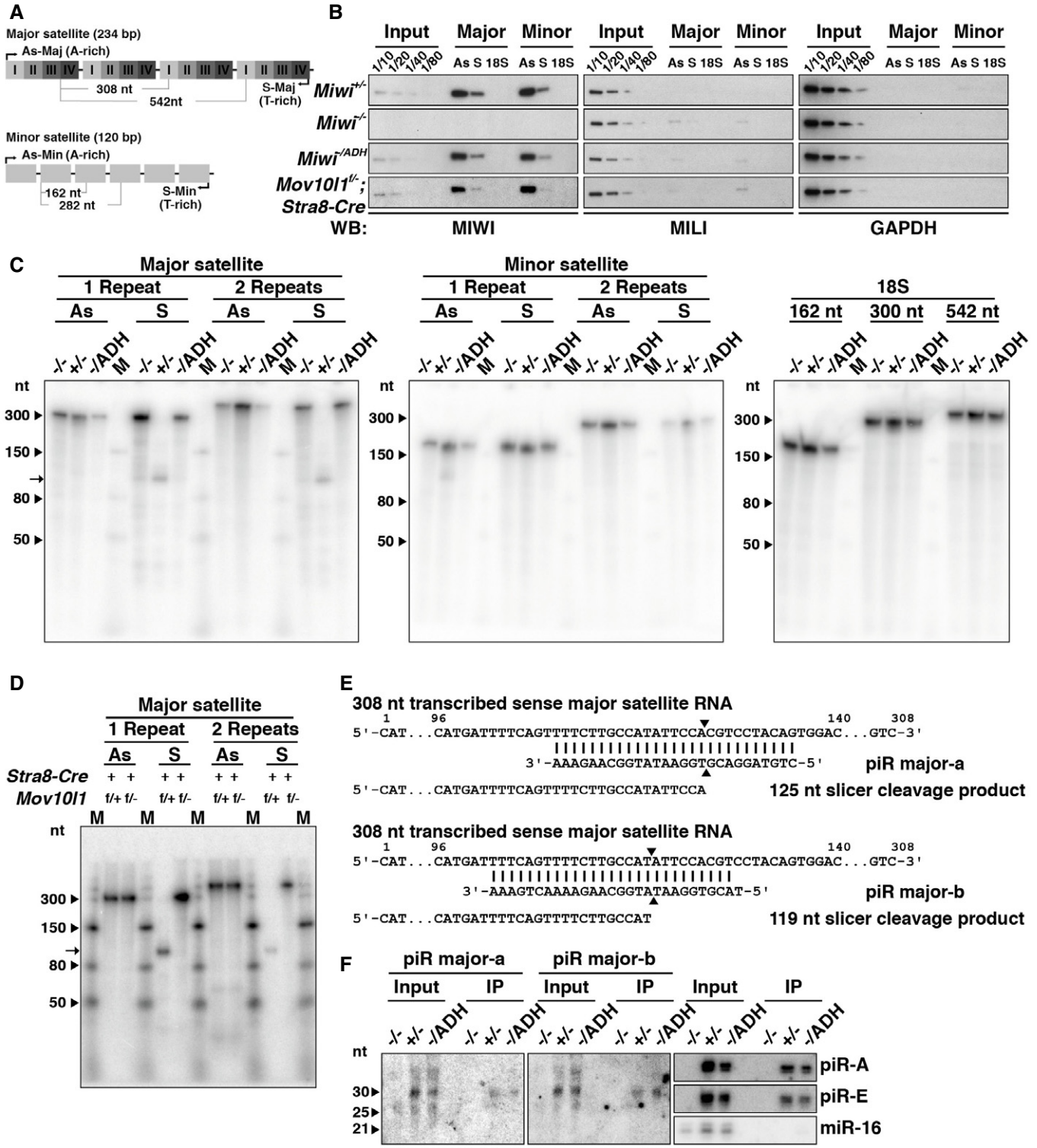

Figure 4.

Furthermore, time course analysis of cleavage reactions by the nuage–nuclear extracts also showed that only *Miwi*$^{+/-}$ cleaved the sense major satellite RNA substrate and that the cleavage increased with increasing incubation time (Appendix Fig S9). These data confirm that MIWI cleaves a specific site on each repeat unit of the sense major satellite transcripts. This *in vitro* assay might not have fully recapitulated MIWI activity *in vivo*, since MIWI is equally required *in vivo* to reduce the expression of all four types of satellite RNAs (Fig 2A). As controls, *in vitro* transcribed 18S rRNA transcripts, equivalent in lengths to the respective satellite RNA

substrates, were not cleaved in all reactions (Fig 4C, right panel). These results indicate the possibility that the slicer activity of MIWI might be specific to satellite RNAs.

To further verify that the *in vitro* cleavage product from the nuage–nuclear extracts is due to MIWI activity but not the other nuclease in the extracts, we repeated the assay using immunopurified FLAG-tagged MIWI protein, with the nuage–nuclear extracts as a control. The FLAG-immuno-purified MIWI generated the same cleavage product as the $Miwi^{+/-}$ extract, but not by the FLAG immune-precipitate from the wild-type testicular extract and the $Miwi^{-/-}$ nuage–nuclear extract failed to generate any cleavage products (Appendix Fig S10A and B). As a further control, antisense major satellite RNAs were not cleaved in all reactions. These results indicate that the *in vitro* cleavage product from sense major satellite RNA substrates is generated by the MIWI activity.

To further compare the nuclease activities of immunopurified MIWI and the nuage–nuclear extract, we conducted *in vitro* RNA processing assay on a 40-nt synthetic RNA substrate bearing complementarity to endogenous piR-A, using either immunopurified MIWI, or nuage–nuclear extracts $Miwi^{+/-}$ or $Miwi^{-/-}$ testes (Appendix Fig S10C). The immunopurified MIWI generated a 26-nt 5′ cleavage product (Appendix Fig S10D), as previously reported (Reuter *et al*, 2011). The $Miwi^{+/-}$ nuage–nuclear extracts generated a 25–27 nt product, but $Miwi^{-/-}$ nuage–nuclear extract showed no detectable nuclease activity (Appendix Fig S10D). As negative controls, there was no same cleavage product in either reaction with immunopurified control or $Miwi^{-/-}$ nuage–nuclear extracts. These data show that there is no other RNase with sequence-specific cleavage activity in nuage–nuclear extracts.

MIWI cleavage of pericentromere-encoded RNA transcripts depends on specific piRNAs

To investigate whether MIWI-mediated sense satellite RNA cleavage depends on pachytene piRNAs, we performed *in vitro* RNA processing assay on spermatocytes from *Mov10l1* heterozygotes or its conditional knockouts. The same cleavage product from one or two repeat units of sense major satellite RNA was detected in lysates from *Mov10l1* heterozygotes but not from *Mov10l1* germline knockouts (Fig 4D). Expectedly, the antisense major satellite RNA substrate was not cleaved in ether reaction. These results indicate that pachytene piRNAs are required for MIWI-mediated cleavage of sense major satellite RNA.

To identify piRNAs involved in sense major satellite RNA cleavage, we examined whether any of the published MIWI-associated piRNAs (Robine *et al*, 2009) is complementary to the sense major satellite RNA and causes its cleavage by MIWI into the observed size. Based on previous observations (Reuter *et al*, 2011), we defined complementary piRNAs as those bearing perfect match from nucleotides 2–22 to the target RNA. Two piRNAs, herein named piR major-a or piR major-b, originated from chr2:98662850 and chr2: 98662847, respectively, are complementary to sense major satellite RNA. Moreover, these piRNAs match the predicted cleavage site of the sense major repeat substrates in the *in vitro* RNA processing assay (Reuter *et al*, 2011; Fig 4E), implicating that these two piRNAs might guide MIWI to the sense major satellite RNAs *in vivo*. Indeed, we are able to detect piR major-a and piR major-b expression *in vivo* by a quantitative stem loop RT–PCR of the 17–35 nt size-selected small RNA pools from MIWI heterozygote and knockout spermatocytes (Appendix Fig S11). Their abundance is approximately 20-fold lower than that of piR-A and piR-E, the two most abundant pachytene piRNAs in wild-type spermatocytes. The presence of piR major-a or piR major-b in spermatocytes supports their involvement in the cleavage of sense major satellite RNA *in vivo*.

To further investigate whether these two piRNAs associate with MIWI *in vivo*, we conducted anti-MIWI immunoprecipitation, followed by small RNA Northern blot analysis of co-precipitated endogenous piRNAs. Both piR major-a and piR major-b, but not miR-16, require MIWI for their biogenesis (Fig 4F, input lanes). However, their biogenesis does not require the MIWI slicer activity (Fig 4F, input lanes), similar to other pachytene piRNAs (Reuter *et al*, 2011). Both piR major-a and piR major-b were immunoprecipitated in lysates from wild-type and MIWI catalytic mutant testes but not from MIWI-depleted testes (Fig 4F). As positive and negative controls, MIWI and its catalytic mutant were able to bind to two other known partner piRNAs, piR-A, and piR-E (Reuter *et al*, 2011), but not miR-16.

To verify the targeting specificity of piR major-a and piR major-b, we first *in vitro* transcribed a 5′-^{32}P-labeled major satellite RNA fragment corresponding to monomers II and III of major satellite sequence (118 nt; Fig EV3A and B) and subjected it to the *in vitro* RNA processing assay to see whether it would generate the predicted cleavage products by piR major-a and major-b as indicated in Fig EV3B. Mixing this fragment with the nuage–nuclear lysate from 21 to 24 dpp $Miwi^{+/-}$ testes yielded a 5′ cleavage product that is ~45 nts (Fig EV3D–F, lane 4), implying that the monomers II and III fragment can be sliced by MIWI-piRNA complex at the piRNA complementary site.

To confirm that piR major-a and major-b are responsible for the targeted cleavage by MIWI, we disrupted the piR major-a and major-b target sequences in monomers II and III DNA template with a 25-nt deletion (Δ25) that disrupts pairing with both of piR major-a and major-b or 10-nt deletions that uncover the 5′-end of piR major-a (Δa), the 5′-end of piR major-b (Δb), or the 3′-end of piR major-a (Δc, Fig EV3C). The Δ25 sense major satellite transcript fragment could no long generate a cleavage product in either MIWI-containing or MIWI-deficient lysate (Δ25; Fig EV3D–F, lanes 7 and 8), validating that piR major-a and piR major-b are required for the cleavage. As additional negative controls, antisense major satellite RNA substrates were not cleaved in ether reaction (Fig EV3D–F, lane 2–3). Furthermore, adding increasing amounts of a 2′-o-methylated 25-nt RNA oligo that competes with piR major-a and major-b combing to the major satellite substrate reduced the cleavage in a dose-dependent manner (Appendix Fig S12). These observations indicate that piR major-a and major-b are responsible for targeting MIWI to the cleavage site.

We noticed that the Δa, Δb, and Δc sense fragments still generated cleavage products that was absent in lysates from MIWI slicer-defective and *Mov10l1* germline knockout testes (Fig EV3E and F, lanes 9–14). Similarly, when we introduced multiple mutations to the RNA substrate that disrupted pairing with both piR major-a and major-b (Appendix Fig S13A, Mt-1, 2, and 3), all of the mutated RNA substrates were still sliced albeit less efficient as compared to the wild-type substrate. The cleavage product was not detected in lysates from *Miwi* homozygote testes. These observations are consistent with previous findings that MIWI-piRNA complex can repress target mRNA via imperfectly base pairing (Reuter *et al*,

2011; Gou *et al*, 2014). In addition, these results imply that it is possible that other piRNAs may exist to guide MIWI to cleave these mutated sense major fragments.

To verify that the observed major satellite RNA fragments are indeed generated by MIWI slicing, we conducted 5′ rapid amplification of cDNA end (5′ RACE) by using two set of sequence-specific primers (Fig EV4A). Both sets amplified 5′ end cDNAs of expected sizes in MIWI heterozygote but not knockout lysate (Fig EV4B). Interestingly, the sequences of 5′ RACE products presented multiple closely nested cleavage sites, including the predicted cleavage sites that were most frequently cleaved (Fig EV4C). This indicates that piR major-a and major-b are mainly responsible for guiding MIWI cleavage and that other piRNAs corresponding to sense major satellite RNAs might exist *in vivo*. To identify these piRNAs, piRNAs from the MIWI-immunoprecipitated small RNA-seq experiments were aligned to the sense and antisense major satellite fragments allowing up to 3 mismatches. This allowed us to identify two more complementary piRNAs, piR major-c and major-as, that bind to MIWI *in vivo* and bear perfect match from nucleotides 2–22 to sense and antisense major satellite RNAs, respectively (Appendix Table S2; Appendix Fig S14). These results indicate MIWI-piRNA complex can target both strands of major satellite RNAs *in vivo* and our *in vitro* RNA processing assay only recapitulated its activity toward the sense strand. However, no complementary piRNA fitting the criteria and corresponding to minor satellites was identified (Appendix Table S2).

MIWI and Dicer cleave the same satellite RNAs

While the sense transcripts of major satellite can be cleaved by MIWI and piRNA-mediated machinery, the discrete cleavage products were not observed in RNA isolated from the testis (Fig 2A). This points to the possibility that other pathways are also involved in satellite RNA processing. Indeed, it has been reported that, in mitosis, centromeric and pericentromeric transcripts are processed by a Dicer-dependent RNAi-like mechanism, which is critical for centromere integrity and chromosome segregation (Fukagawa *et al*, 2004; Kanellopoulou *et al*, 2005; Murchison *et al*, 2005; Eymery *et al*, 2009a; Huang *et al*, 2015). In the male germline, Dicer is known to participate in multiple developmental events, including primordial germ cell proliferation, meiotic prophase I, and spermatid elongation (Hilz *et al*, 2016). Deletion of Dicer in germ cells from postnatal day 3 or 5 onwards leads to aberrant expression of pericentromeric major satellite transcripts, an increased number of apoptotic spermatocytes and infertility (Korhonen *et al*, 2011; Greenlee *et al*, 2012). To investigate the possible role of Dicer in satellite RNA turnover, we conducted the RNA pull-down assay. Dicer was precipitated by major and minor satellite RNAs even in absence of MIWI, its catalytic mutant, or mature piRNAs (Fig 5A and Appendix Fig S7). To further verify whether Dicer interacts with both strands of satellite RNAs *in vivo*, we conducted Dicer-RNA co-immunoprecipitation assay. Dicer was associated with both strands of all satellite RNAs *in vivo* in either $Miwi^{+/-}$ or $Miwi^{-/-}$ background (Fig EV5A). These results indicate that Dicer binds to satellite RNAs independently of MIWI-piRNA complexes, consistent with the previous finding that MIWI is not required for Dicer stability and functional activity (Grivna *et al*, 2006b). The association of Dicer with both strands of major satellite RNAs is reduced in $Miwi^{-/-}$ testis, indicating the possibility that MIWI might facilitate Dicer binding to the major satellite transcripts.

To further address the functional relationship between Dicer and MIWI in regulating satellite RNA turnover, we knocked out *Miwi*, *Dicer*, and both *Miwi* and *Dicer* in postnatal male germ cells (Materials and Methods; Fig 5B), and examined the satellite RNA expression in these mice by Northern blot and quantitative RT–PCR analyses. As reported in Fig 2A, both sense and antisense strands of major satellite transcripts are over-expressed in $Miwi^{-/-}$ spermatocytes (Figs 5B and EV5B), indicating the function of MIWI in promoting satellite RNA turnover. Notably, Dicer deletion also caused an obvious enrichment of both sense and antisense strands of major and minor satellite transcripts, indicating that Dicer is also involved in both major and minor satellite RNA processing. Most importantly, satellite transcripts were most over-expressed when MIWI and Dicer were both deleted. This reflects an additive effect between MIWI and Dicer in processing satellite RNAs.

Noticeably, both strands of the accumulated major satellite transcripts were up-shifted to larger sizes in the double knockout spermatocytes (Fig 5B). This indicates that the processing of major satellite transcripts may be different from that of minor satellite transcripts and that both sense and antisense major satellite transcripts are target of MIWI-piRNA complex *in vivo*, which is consistent with previous results (Appendix Table S2 an Appendix Fig S14).

To dissect how MIWI and Dicer are involved in processing satellite transcripts, we repeated the *in vitro* RNA processing assay for sense major transcripts in Fig 4C using spermatogenic lysates that contain MIWI, Dicer, or both. To this end, we first validated that the 21–24 dpp nuage–nuclear extracts contained MIWI but not Dicer by Western blot analysis (Appendix Fig S8B). To be absolutely definitive that our nuage–nuclear preparations are free of even a trace amount of Dicer that was undetected by Western blotting, we prepared $Miwi^{+/-}$ nuage–nuclear extracts from *Dicer*-null spermatocytes, with $Dicer^{+/-}$;$Miwi^{+/-}$ and $Dicer^{+/-}$;$Miwi^{-/-}$ extracts as controls (Fig 5C). $Miwi^{+/-}$ extracts, either $Dicer^{+/-}$ or *Dicer*-null, but not *Miwi*-null extracts, cleaved sense but not antisense major satellite transcripts to smaller fragments (Fig 5C). These results reflect that the cleavage of the sense major satellite transcripts by MIWI-piRNA complexes does not depend on Dicer.

To further dissect how MIWI and Dicer may work together in processing major satellite RNAs, we first investigated whether the MIWI-piRNA complex cleaves sense and antisense satellite RNA substrates into shorter fragments to promote dsRNA formation, which would be favorable substrates for Dicer (Vermeulen *et al*, 2005). Total RNAs from $Miwi^{+/-}$;$Dicer^{f/+}$;*Stra8-Cre*, $Miwi^{-/-}$;$Dicer^{f/+}$;*Stra8-Cre*, $Miwi^{+/-}$;$Dicer^{f/-}$;*Stra8-Cre*, and $Miwi^{-/-}$;$Dicer^{f/-}$;*Stra8-Cre* spermatocytes were digested by either dsRNA-specific endoribonuclease RNase III or single-strand-specific endonuclease nuclease S1 and then subjected to Northern blot assay. Without MIWI and Dicer, both long single-stranded satellite RNA (RNase III-resistant; mostly > 6 Kb) and short double-stranded satellite RNA (Nuclease S1-resistant, mostly 0.1–1.5 kb) are accumulated (Fig 5D). Adding MIWI eliminated the long ssRNAs where the short dsRNA species remain accumulated; whereas adding Dicer almost completely eliminated the dsRNAs while the long ssRNAs were still accumulated. Only when MIWI and Dicer are both present, both the long ssRNA and short dsRNA populations are almost completely eliminated. These results support the notion that the MIWI-piRNA

complex processes long satellite ssRNAs to facilitate their formation of shorter dsRNA fragments for further digestion by Dicer. As negative controls, the processing of 18S and 28S rRNAs was not affected in either *Miwi* or *Dicer* mutant, indicating that the MIWI/Dicer-mediated satellite RNA processing pathway is not a general pathway that is involved in processing some other repetitive RNAs.

To verify that Dicer can further process major satellite RNA fragments generated by MIWI-piRNA complex, we conducted a sequential

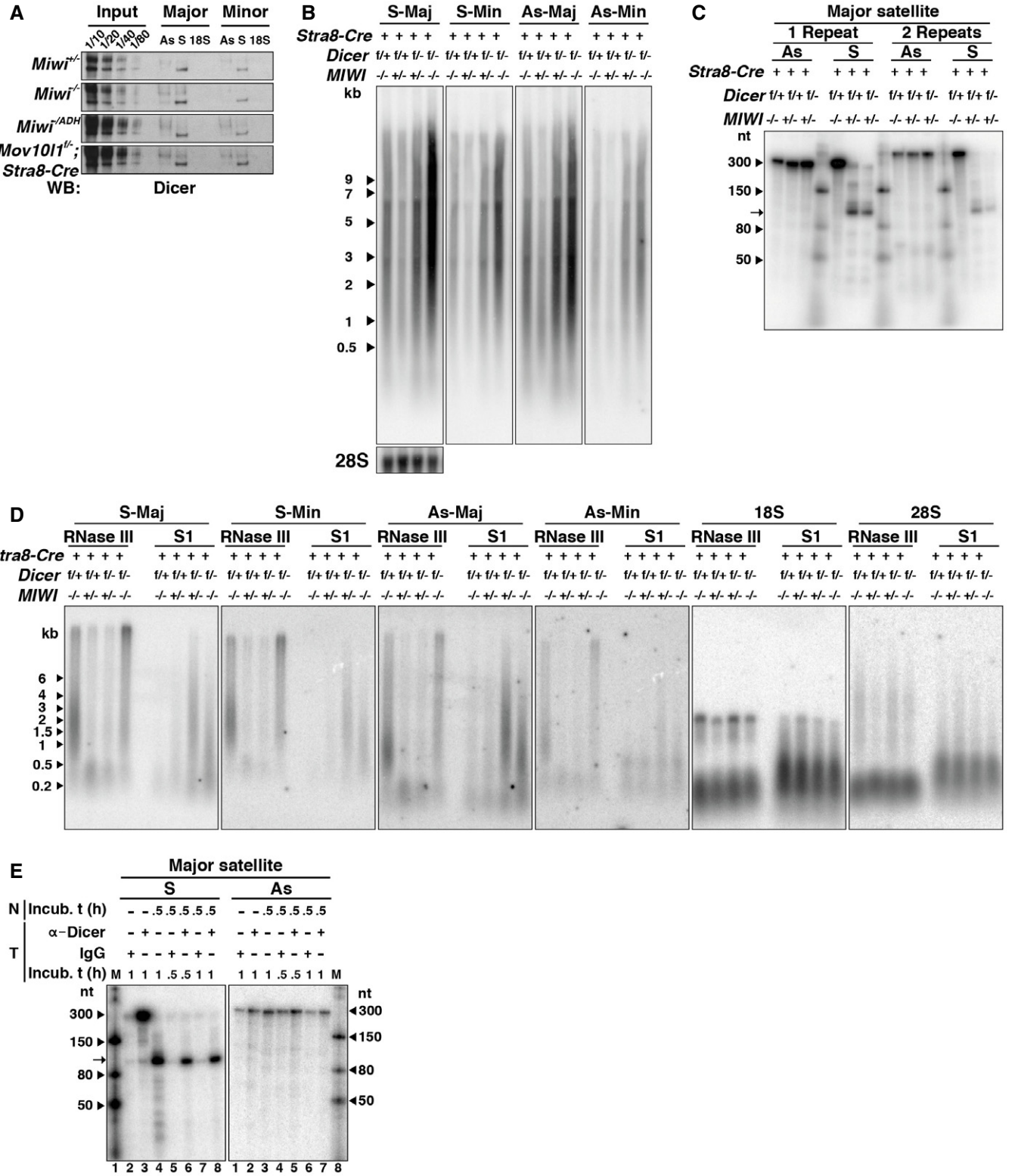

Figure 5.

Figure 5. MIWI works with Dicer to ensure proper satellite RNA processing.

A RNA pull-down was performed using *in vitro* transcribed biotinylated transcripts and whole-cell extracts from *Miwi*$^{+/-}$, *Miwi*$^{-/-}$, *Miwi*$^{-/ADH}$, and *Mov10l1*$^{f/-}$;*Stra8-Cre* testes. *Mov10l1*$^{f/-}$;*Stra8-Cre* mice represent a pachytene piRNA-deficient condition. *In vitro* transcribed RNAs corresponding to approximately one repeat of major and minor satellite sequences were used as baits. Precipitated protein was visualized by Western blotting using anti-Dicer antibody.

B Equal amounts of total RNA isolated from spermatocytes of *Miwi*$^{+/-}$;*Dicer*$^{f/+}$;*Stra8-Cre*, *Miwi*$^{-/-}$;*Dicer*$^{f/+}$;*Stra8-Cre*, *Miwi*$^{+/-}$;*Dicer*$^{f/-}$;*Stra8-Cre*, and *Miwi*$^{-/-}$;*Dicer*$^{f/-}$;*Stra8-Cre* mice were resolved on a 1% agarose gel. The gel was subjected to Northern blot analysis using probes specific for the sense and antisense sequences of major and minor satellites. The blot was re-hybridized with a 28S rRNA-complementary probe to demonstrate equal loading (bottom on the left).

C *In vitro* RNA processing assay with nuage-enriched nuclear fraction from *Miwi*$^{+/-}$;*Dicer*$^{f/+}$;*Stra8-Cre*, *Miwi*$^{-/-}$;*Dicer*$^{f/+}$;*Stra8-Cre*, and *Miwi*$^{+/-}$;*Dicer*$^{f/-}$;*Stra8-Cre* mice, and 5′-end radioactively labeled RNA targets corresponding to approximately one and two repeats of sense and antisense major satellite sequences. Arrow indicates the cleavage products of *In vitro* transcribed sense major satellite RNAs by MIWI-piRNA complex.

D Equal amounts of total RNA isolated from spermatocytes of *Miwi*$^{+/-}$;*Dicer*$^{f/+}$;*Stra8-Cre*, *Miwi*$^{-/-}$;*Dicer*$^{f/+}$;*Stra8-Cre*, *Miwi*$^{+/-}$;*Dicer*$^{f/-}$;*Stra8-Cre*, and *Miwi*$^{-/-}$;*Dicer*$^{f/-}$;*Stra8-Cre* mice were digested with RNase III (RNase III) or nuclease S1 (S1), and further resolved on a 1% agarose gel. The gel was subjected to Northern blot analysis using probes specific for the sense (S) and antisense (As) strands of major (Maj) and minor (Min) satellite transcripts. The blot was re-hybridized with 18S and 28S complementary probes to demonstrate equal loading and the same efficiency of RNase III or nuclease S1 digestion.

E Sequential *in vitro* RNA processing assay using 5′-end radioactively labeled RNA targets corresponding to approximately one repeat of sense and antisense major satellite sequences. The nuage–nuclear fraction from *Miwi*$^{+/-}$ testes is indicated as N. Total cellular extracts (T) from *Miwi*$^{+/-}$ testes were subjected to immunodepletion using anti-Dicer antibodies (α-Dicer), with IgG (IgG) as a negative control. The incubation time (Incub. t) was 0.5 and 1 h. The arrow indicates the product of MIWI-mediated cleavage of the *in vitro* transcribed sense major satellite RNA.

Source data are available online for this figure.

cleavage analysis. We first incubated the one repeat sense and antisense major satellite RNA substrates with 21–24 dpp nuage–nuclear extracts (N) for half hour to allow MIWI to cleave the RNAs (Fig 5E). The same substrates without incubating with the nuage–nuclear extracts were used for the subsequent step as a negative control for MIWI cleavage. We then added 21–24 dpp total cellular extracts (T) to introduce Dicer activity and incubated the substrates with the extracts for 0.5 and 1 h to examine how the MIWI cleavage products would be processed by Dicer. As a negative control for Dicer activity, the total cellular extract was replaced by its buffer, followed by the same time of incubation. As a second negative control for Dicer activity, total cellular extract was immunodepleted to remove endogenous Dicer by adding anti-Dicer antibody and then precipitating it (α-Dicer), yet as a control for possible nonspecific effect of the anti-Dicer antibody, IgG instead of the antibody was added to the total cellular extract for the assay (IgG). Fig 5E shows that Dicer cleaved sense RNA that had not been cleaved by MIWI (left penal, lane 2) as well as MIWI cleavage products (left penal, lanes 5 and 7), as judged by a decrease of the full-length substrates in these lanes. Thus, Dicer can act independent of MIWI in cleaving the sense RNA substrate. In addition, these results are consistent with our observation that MIWI association with Dicer is RNA- but not piRNA-dependent (Fig EV5C and D), as revealed by immunoprecipitation assay. Thus, MIWI and Dicer may interact with the same RNA target. Moreover, unlike MIWI, Dicer cleaved the antisense RNA substrate, as indicated by proportionally decreased levels of the antisense RNA substrates with 0.5 and 1 h with the total cellular extracts (Fig 5E, right penal, lane 4–7). Adding anti-Dicer antibodies partially prevented the decrease, implying that observed processing is at least partially due to Dicer activity. These results support the idea that the MIWI-piRNA complex and Dicer both cleave the same major satellite RNAs and that Dicer further processes the MIWI cleavage product.

Proper satellite RNA processing is correlated to proper chromosome segregation

To investigate the biological significance of MIWI-Dicer action in processing satellite RNAs, we assessed the effects of their removal on the progression and fidelity of meiotic division. We first examined the architecture of sister kinetochores in *Miwi*$^{-/-}$, *Dicer*$^{-/-}$, and *Miwi*$^{-/-}$;*Dicer*$^{-/-}$ MI spermatocytes, with *Miwi*$^{+/-}$;*Dicer*$^{+/-}$ as a positive control. Combined immunofluorescence and DNA FISH experiments revealed that *Miwi*$^{-/-}$ and *Dicer*$^{-/-}$ spermatocytes contain a significantly reduced number of normal sister kinetochore pairs that have overlapping inner plates, as compared to *Miwi*$^{+/-}$;*Dicer*$^{+/-}$ spermatocytes. The frequency of normal sister kinetochore pairs was the lowest in *Miwi*$^{-/-}$;*Dicer*$^{-/-}$ spermatocytes (Fig 6A). Correspondingly, the frequencies of abnormal sister kinetochores with adjacent or separated inner plates in *Miwi*$^{-/-}$ and *Dicer*$^{-/-}$ spermatocytes were significantly higher than that of *Miwi*$^{+/-}$;*Dicer*$^{+/-}$ spermatocytes. This frequency was the highest among *Miwi*$^{-/-}$;*Dicer*$^{-/-}$ spermatocytes. We then further examined the outer plate alignment of the sister kinetochores, which showed the same trend (Fig 6B). These results indicate that both MIWI and Dicer contribute to proper sister chromatid cohesion in an additive manner, and that the frequency of abnormal kinetochore pairs was proportional to the levels of satellite transcript over-expression (Fig 5B) in the corresponding genotypes.

Consistent with these observations (Fig 6A and B), *Miwi*$^{-/-}$, *Dicer*$^{-/-}$, and *Miwi*$^{-/-}$;*Dicer*$^{-/-}$ MI spermatocytes displayed correspondingly increased frequencies of chromosome misalignment as compared to *Miwi*$^{+/-}$;*Dicer*$^{+/-}$ spermatocytes, with *Miwi*$^{-/-}$;*Dicer*$^{-/-}$ spermatocytes showing the highest frequency of chromosome misalignment (Fig 6C). Although this had no immediate impact on the chromosomal complement in MI spermatocytes (Fig 6D), it led to correspondingly higher frequencies of aneuploidy in MII spermatocytes (Fig 6E) and increased cell death in meiotic metaphase in these genotypes (Appendix Fig S15). These results reveal that the combined action of the MIWI-piRNA complex and Dicer in processing satellite transcripts in mouse spermatocytes is important for meiotic kinetochore establishment and, consequently, faithful chromosome segregation during meiosis.

Discussion

Although MIWI is well known to play a major role in pachytene piRNA biogenesis during meiosis and in spermiogenesis (Deng &

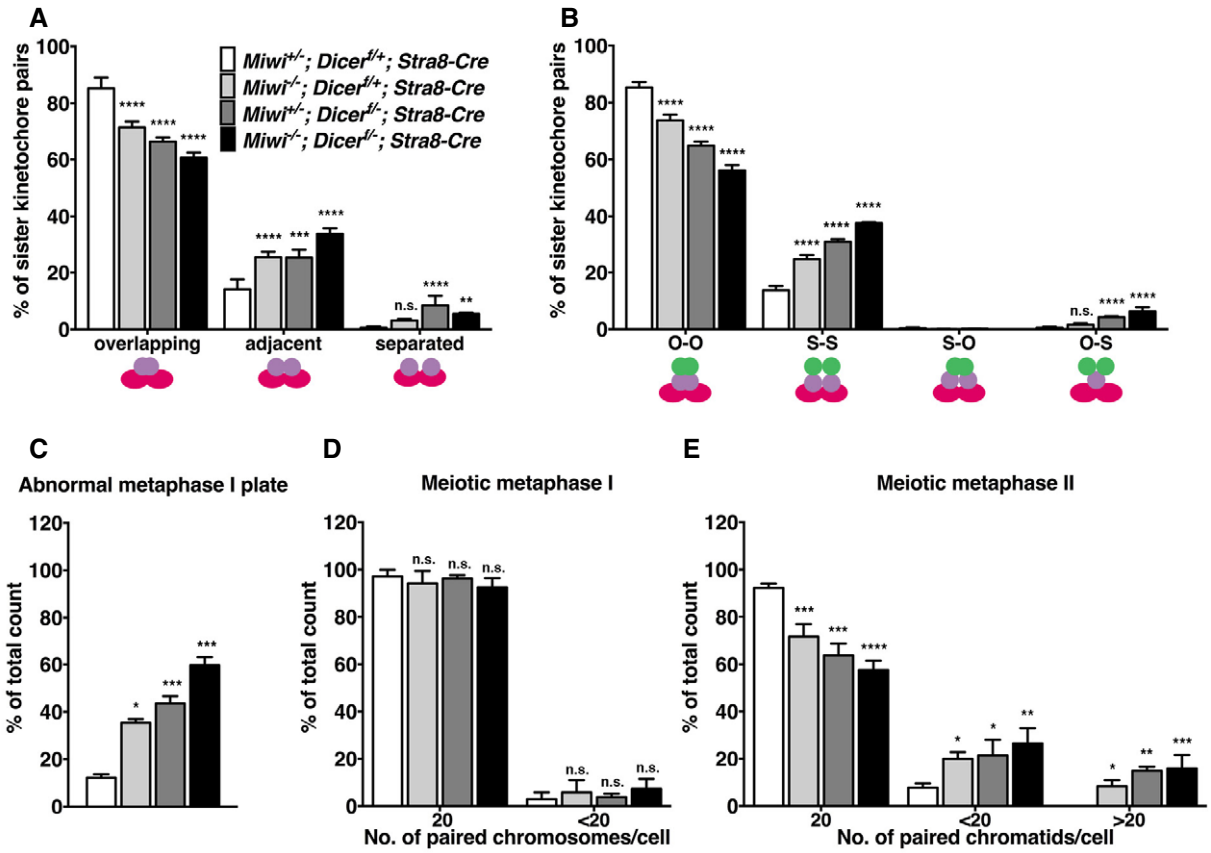

Figure 6. The effects of removing MIWI and Dicer on the progression and fidelity of meiotic division.

A Frequency of overlapping, adjacent, and separated inner kinetochores. Spermatocytes from *Miwi*$^{+/-}$;*Dicer*$^{f/+}$;*Stra8-Cre*, *Miwi*$^{-/-}$;*Dicer*$^{f/+}$;*Stra8-Cre*, *Miwi*$^{+/-}$;*Dicer*$^{f/-}$;*Stra8-Cre*, and *Miwi*$^{-/-}$;*Dicer*$^{f/-}$;*Stra8-Cre* mice were used to examine sister kinetochore configuration at meiosis I as shown in Fig 3A and B. n = 3 mice for each genotype. The total numbers of counted cells in the four types of spermatocytes were 101, 117, 129, and 115, respectively. The total numbers of counted sister kinetochore pairs in the four types of spermatocytes were 4,040, 4,680, 5,160, and 4,600, respectively.

B Frequency of the different sister kinetochore configurations. The four types of spermatocytes in A were used to examine sister kinetochore configurations in meiosis I metaphase with O-O, S-S, O-S, or S-O as defined in the text. n = 3 mice for each genotype. The total numbers of counted cells in the four types of spermatocytes were 134, 140, 140, and 130, respectively. The total numbers of counted sister kinetochore pairs in the four types of spermatocytes were 5,360, 5,600, 5,600, and 5,200, respectively.

C Frequency of abnormal arrangement in the meiotic metaphase I plate. The four types of spermatocytes in A and B were used to perform immunofluorescence as shown in Fig 1B and C. n = 3 mice for each genotype. The total numbers of counted metaphase I plates in the four types of spermatocytes were 221, 181, 421, and 240, respectively.

D Frequency of meiosis I metaphase cells with chromosomal abnormalities. The four types of spermatocytes in A-C were used to perform a metaphase spread as shown in Fig 1H and I. n = 3 mice for each genotype. The total numbers of counted MI cells in the four types of spermatocytes were 89, 73, 132, and 104, respectively.

E Frequency of meiosis II metaphase cells with chromosomal abnormalities. The four types of spermatocytes in A-D were used to perform a metaphase spread as shown in Fig 1K and L. n = 3 mice for each genotype. The total numbers of counted MII cells in the four types of spermatocytes were 74, 87, 85, and 94, respectively.

Data information: The results represent the mean ± SD of at least three independent experiments. The statistical test was assessed using one-way ANOVA test (*P < 0.05; **P < 0.01; ***P < 0.001; ****P < 0.0001; n.s., P > 0.05).
Source data are available online for this figure.

Lin, 2002), its meiotic function remains unknown (Reuter *et al*, 2011; Watanabe *et al*, 2015). In this study, we report a key function of MIWI during meiosis for the faithful segregation of chromosomes. Furthermore, we provide strong evidence implicating that the MIWI-piRNA complex achieves this function by processing pericentromere-encoded major satellite RNAs to prevent their over-accumulation, which in turn ensures the centromere cohesion and kinetochore assembly of sister chromatids during meiosis I and thus prevent their mis-segregation during meiosis. Finally, we show that Dicer is also involved in processing the satellite RNAs and work together with the MIWI-piRNA pathway to ensure proper chromosome segregation during meiosis. These discoveries illustrate the crucial role of the PIWI-piRNA pathway in kinetochore assembly and meiosis.

The role of MIWI and Dicer in maintaining the homeostasis of satellite transcripts and chromosome segregation during meiosis

A robust role of satellite RNA processing in somatic, meiotic, and embryonic stem cells has previously been ascribed to Dicer

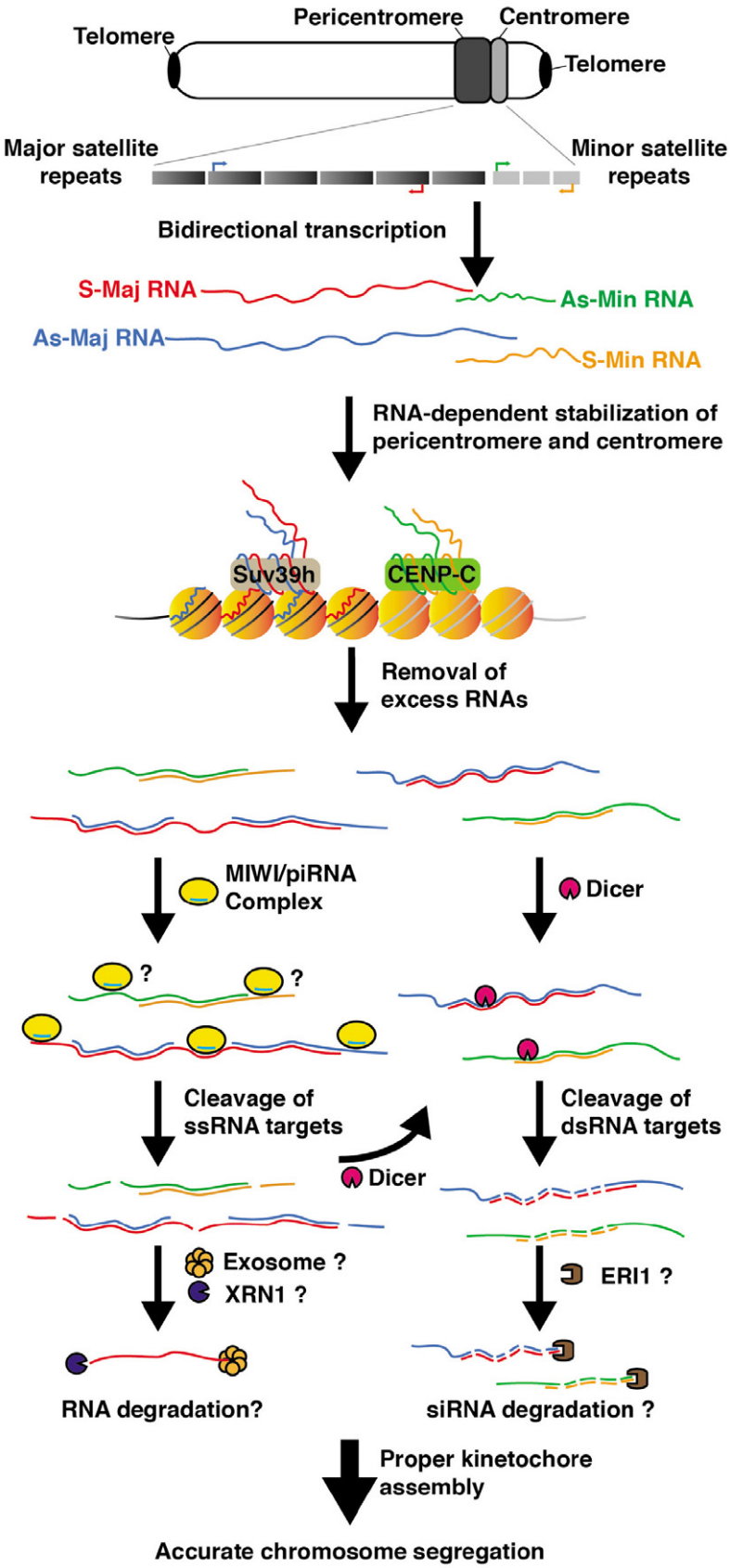

Figure 7.

Figure 7. Pathway that reduces satellite transcripts in male meiosis.

Schematic diagram showing location of major and minor satellite repeats at pericentric heterochromatin and centric heterochromatin on a mouse chromosome (upper) and organization of mouse major and minor satellite repeats (gray and light gray, respectively). During premeiotic DNA replication and meiotic DNA prophase I, spermatocytes bidirectionally transcribe the long and heterogeneous transcripts encoded by major and minor satellite DNA. The resulting major satellite transcripts associate with nucleosomes and Suv39 h, and hybridize with major satellite repeats to stabilize pericentric heterochromatin, which allows faithful kinetochore assembly. Meanwhile, minor satellite transcripts stabilize DNA-binding of CENP-C to complete the centromere identity. To remove excess satellite transcripts, double-stranded satellite transcripts are sliced by Dicer-mediated processing and might be followed by ERI1-mediated siRNA degradation. Meanwhile, single-stranded major satellite transcripts are recognized by MIWI-piRNA complexes and processed to smaller fragments that can effectively form double-stranded RNA with their complementary satellite RNA sequence for Dicer degradation. Alternatively, these smaller fragments could be degraded by the 5′-to-3′ exoribonuclease XRN1 and the exosome. Consequently, spermatocytes can keep a suitable amount of satellite transcripts for proper kinetochore assembly and normal chromosome segregation during meiotic metaphase I. S, sense; As, antisense; Maj, major satellite; Min, minor satellite; CENP-C, centromere protein c; ERI1, enhanced RNAi-1.

(Fukagawa *et al*, 2004; Kanellopoulou *et al*, 2005; Murchison *et al*, 2005; Hsieh *et al*, 2011; Korhonen *et al*, 2011; Huang *et al*, 2015). During mitosis, the bidirectional transcription of satellite RNAs occurs during DNA replication and their appropriate expression stabilizes the overall kinetochore structure in G2/M phase (Ferri *et al*, 2009; Gent & Dawe, 2012). However, in mice, it takes 10 days for meiotic prophase I to progress from preleptotene to diakinesis/metaphase I (Goetz *et al*, 1984), yet transcription mostly occurs during the mid-pachytene stage (Hecht, 1986). Therefore, the regulation of major satellite transcripts in male meiotic cells may be different from mitotic cells (Rudert *et al*, 1995). Notably, mammals do not have an RNA-dependent RNA polymerase that converts the single-stranded RNAs (ssRNAs) to double-stranded RNA (dsRNA) intermediates to be cleaved by Dicer. Therefore, they presumably need another mechanism to convert ssRNAs to dsRNAs for Dicer cleavage. Our findings indicate that the MIWI-piRNA complex might increase the amount of dsRNA substrates for Dicer during male meiosis. MIWI cleaves major satellite transcripts through piRNA-guided slicing (Figs 4, 5B–D, EV3, EV4, and Appendix Fig S10, S12 and S13). The ssRNA cleavage products, now much shorter, can more effectively form dsRNAs with their complementary major satellite RNAs (Fig 5E). This is especially possible because major satellite RNAs are composed of a common heterotetrameric repeats, each of which contain four different 58–60 bp monomers (Abdurashitov *et al*, 2009). Thus, the MIWI-fragmented T-rich sense transcripts can easily form a double-strand form by annealing with many of its complementary A-rich sequences in antisense major transcripts. Similarly, MIWI-piRNA complex may slice antisense major transcripts to form a double-strand form of satellite RNA (Fig 5D, Appendix Table S2, Appendix Fig S10 and S14). However, we cannot rule out the possibility that MIWI-piRNA complex could slice both strands of major satellite RNAs because these RNAs contain less ordered repeats that may be arranged by head-to-tail orientation, as in fission yeast and human (Fishel *et al*, 1988; Aldrup-Macdonald & Sullivan, 2014). Therefore, our findings imply that MIWI facilitates Dicer-mediated post-transcriptional machinery to process major satellite RNA transcripts, forming a meiosis-specific strategic alliance for proper assembly of kinetochore and faithful chromosome segregation. The production of 21-nt small RNAs corresponding to satellite RNAs was not observed (Appendix Fig S16), implying that other downstream degradation might exist, such as 3′-to-5′ exoribonuclease ERI1 (enhanced RNAi-1) that is expressed in the testis (see *the Human Protein Atlas*) to negatively regulate the activity of miRNA/siRNA-mediated gene repression by degrading siRNA-containing duplexes (Almeida *et al*, 2006; Bian *et al*, 2011; Thomas *et al*, 2012, 2014).

Possible roles of MIWI in processing minor satellite transcripts

Our results show that both MIWI and Dicer pathways have similar functions in preventing the over-accumulation of minor satellite RNAs, yet through different modes of action. Dicer associates with sense and antisense minor satellite RNAs independent of MIWI and piRNA (Figs 5A and EV5A). Dicer deficiency leads to the over-accumulation of these RNAs (Fig 5B). This is consistent with previous observations that Dicer-mediated post-transcriptional regulation is required to diminish both major and minor satellite transcripts in humans and mice during mitosis (Fukagawa *et al*, 2004; Kanellopoulou *et al*, 2005; Korhonen *et al*, 2011; Huang *et al*, 2015). MIWI, on the other hand, binds to both sense and antisense minor satellite RNAs *in vitro* (Fig 4B) yet does not cleave them (Fig 4C). Despite this, these RNAs are also over-accumulated in *Miwi* mutants (Figs 2A and 5B), which indicates that MIWI may be indirectly involved in processing minor satellite RNAs. Therefore, it is possible that Dicer is directly involved in minor satellite RNA processing yet the MIWI-piRNA pathway helps Dicer in processing minor satellite RNAs by reducing its commitment in processing major satellite RNAs, so that an approximately twofold to threefold accumulation of major satellite transcripts caused by MIWI deficiency affects the processing efficiency of Dicer and thus leads to the overall accumulation of all satellite transcripts. Alternatively, it is possible that MIWI recruits an additional RNA degradation mechanism to these minor satellite transcripts. Indeed, it has been reported that both TRAMP and exosome degrade centromeric transcripts in *S. pombe* during meiosis (Buhler *et al*, 2007; Wang *et al*, 2008). These possibilities await further investigation.

Pathways that eliminate the satellite transcripts in male meiosis

Our findings relate satellite RNAs, MIWI, piRNA, and Dicer in meiotic chromosome segregation and imply their following roles (Fig 7): The MIWI-piRNA complex works with Dicer to process major and minor satellite transcripts, which is essential for proper kinetochore assembly to maintain pericentric heterochromatin (Velazquez Camacho *et al*, 2017), establish centromere identity, and recruit chromosomal passenger complex to centromeres (Chan & Wong, 2012). The over-accumulation of satellite transcripts causes mis-localization of centromere-associated proteins, leading to defects in chromosome segregation and aneuploidy (Fig 2C–I and Appendix Fig S4) (Bouzinba-Segard *et al*, 2006; Hsieh *et al*, 2011; Huang *et al*, 2015; Grenfell *et al*, 2016). In order to remove the excess RNAs, complementary double-stranded satellite RNAs are processed to small-interfering RNAs (siRNAs) by Dicer

(Kanellopoulou *et al*, 2005; Murchison *et al*, 2005; Korhonen *et al*, 2011) and may be further degraded by the 3′-to-5′ exoribonuclease ERI1 (enhanced RNAi-1) that is expressed in the testis (see *the Human Protein Atlas*) to negatively regulate the activity of miRNA/siRNA-mediated gene repression by degrading siRNA-containing duplexes (Almeida *et al*, 2006; Bian *et al*, 2011; Thomas *et al*, 2012, 2014). Moreover, major satellite transcripts can be processed by MIWI-piRNA complexes through piRNA-mediated sequence-specific recognition (Fig 4). The cleavage products may form dsRNAs with their complementary transcripts to serve as substrates for Dicer (Fig 5D) and 5′-to-3′ exoribonuclease Xrn1 or exosome (Orban & Izaurralde, 2005). These pathways maintain satellite transcripts at suitable levels to ensure proper kinetochore assembly and accurate chromosome segregation during male meiosis.

Materials and Methods

Ethics statement

Animal experiments in this study were carried out in accordance with the Animal Use Protocols as approved by the Institutional Animal Care and Use Committee, Yale University (IACUC Protocol number: 2009–11087).

Isolation of MIWI-expressing spermatocytes by fluorescence-activated cell sorting (FACS)

Testes were collected from 21 to 24 dpp mice, tunica albuginea was removed, and tissue was incubated with digestion buffer (0.5 mg/ml collagenase type IV, 0.05% and trypsin–EDTA in DMEM) for 10 min at 37°C, followed by pipetting to release the cells and then added 10% volume of fetal bovine serum (FBS) to stop the reaction. Cells were filtered through a 70-μm cell strainer (BD Falcon) and washed with 1× PBS once and resuspended to obtain single-cell suspensions. For FACS, cell pellets were resuspended with 0.5% FBS and 1 μg/ml PI in DMEM. The *Miwi-GFP* knock-in mice were previously generated in which MIWI ORF is partially replaced by GFP ORF in *Miwi* mutant allele (Deng & Lin, 2002). To collect MIWI-expressing spermatocytes, cells were analyzed on a BD FACSAriaII according to GFP expression level and cell size. Sorted cells were collected by centrifugation at 500 *g* for 5 min and then subjected to further experiments.

Preparation of crude subcellular fractionations and Western blot analysis

Single-cell suspensions from testes were prepared as described above. Whole-cell extracts (WCE) were prepared using WCE buffer (20 mM HEPES, pH 7.4, 0.2 M NaCl, 0.5% Triton X-100, 5% glycerol, 1 mM EDTA, 1 mM EGTA, 10 mM β-glycerophosphate, 2 mM Na_3VO_4, 1 mM NaF, 1 mM DTT, and the protease inhibitor cocktail by Roche). Cells were washed twice in 1× PBS, lysed by trituration through a 25-gauge needle 10 times on ice, rotated for 30 min at 4°C, and centrifuged (21,000 *g*, 30 min, 4°C) to obtain whole-cell extracts. To prepare subcellular fractionations, cell pellets were resuspended in 1 ml of hypotonic buffer (10 mM Tris–HCl pH 7.4, 10 mM NaCl, 3 mM $MgCl_2$, 0.2% NP-40, and the Roche protease inhibitor cocktail) per 10^7 cells. After 10-min incubation on ice, nuclei were collected by centrifugation at 500 *g* for 5 min. The supernatant was centrifuged further at 10,000 g for 10 min to obtain the cytosolic fraction. Nuclei were washed with hypotonic buffer devoid of NP-40 and then resuspended in WCE buffer and centrifuged at 21,000 *g* for 30 min to obtain the nuage–nuclear fraction. Lysates were boiled in 5× loading buffer (250 mM Tris–HCl, pH 6.8, 10% SDS, 0.05% bromophenol blue, 50% glycerol, 25% β-mercaptoethanol) and then fractionated by SDS–PAGE. Western blot analysis was performed after electrophoretic separation of polypeptides by 4–15% SDS–PAGE (Bio-Rad) and transfer to Immobilon-P/PVDF membrane (Millipore). Blots were probed with the indicated primary and appropriate secondary antibodies. Immunobands were subsequently detected by the enhanced chemiluminescence reaction (Pierce).

Indirect immunofluorescence and TdT-mediated dUTP nick end labeling (TUNEL) assay

MIWI-expressing spermatocytes isolated though FACS or purified nuclei were prepared as described above. Cells or nuclei were resuspended in 1× PBS at a final concentration of 5×10^4 cells/100 μl or 1×10^5 nuclei/100 μl, and then centrifuged (500 *g*, 5 min) onto X-tra® Slides (Leica) using cytospin, as described previously (Koh, 2013). After the slides were completely air-dried, cells were fixed in 4% paraformaldehyde (PFA) in 1× PBS and subsequently permeabilized with 0.5% Triton X-100/0.1% Tween-20/1× PBS at room temperature for 20 min. Cells were then blocked in blocking buffer (10% normal goat serum in 1× PBS) and incubated overnight with the indicated primary antibodies in 10% NGS in 1× PBS. Mouse monoclonal anti-phosphor-histone H3 (Ser10) (Cell Signaling 9706, 1:200) and rabbit polyclonal anti-α/β-tubulin (Cell Signaling 2148, 1:100) antibodies were used. Slides were washed three times in 1× PBS and then incubated for 1 h at room temperature in 10% NGS, in 1× PBS containing the relevant secondary antibodies conjugated to Ig-Alexa Fluor 555 or Ig-Alexa Fluor 488 (1:500 dilutions; Invitrogen). Slides were washed three times in PBS, stained with 4′,6-diamidino-2-phenylindole dihydrochloride (DAPI), and then mounted with Vectashield (Vector Labs). Images were photographed using a Zeiss Axio scope microscope and assembled using Zeiss AxioVision software.

For the TUNEL assay, testes were fixed in 4% paraformaldehyde at 4°C overnight, washed with 70% ethanol for 24 h, and embedded in paraffin. TUNEL assays on testis sections were performed using an ApopTag® Fluorescein *In Situ* Apoptosis Detection Kit (Millipore) following the manufacturer's instructions. Images were capture on a Leica TCS SP5 spectral confocal microscope. Image overlays were colored by computer-assisted management of confocal microscopy data generated with Leica Application Suite software.

Preparation of metaphase chromosome spreads

The preparation of metaphase chromosome spreads was carried out as previously described (Deng *et al*, 2003). Single-cell suspensions from 21 to 24 dpp testes were pelleted, washed twice in 1× PBS, and subsequently treated with hypotonic buffer (12.3 mM HEPES, pH 7.5, 0.53 mM EGTA, 64.4 mM KCl) for 20–30 min at 37°C. After hypotonic treatment, cells were prefixed with 50% (final

concentration) of the fixative (3:1 methanol: acetic acid) for 10 min. The cells were collected by centrifugation (300 *g*, 10 min) and washed with the fixative for 10 min four times. After the final centrifugation, the supernatant was removed completely, and the cell pellet was resuspended in 100 μl of the fixative. 10 μl of cell suspension was dropped onto the slide from a height of 1 cm. After the slide dried, the chromosome spreads were stained with DAPI and then analyzed under a phase-contrast microscope (Leica DMI6000 B-inverted fluorescence microscope). Images were colored using Leica Application Suite software.

Combined RNA and DNA fluorescence *in situ* hybridization (FISH)

Single-cell suspensions from 21 to 24 dpp testes were pelleted, washed twice in PBS, and subsequently treated with hypotonic buffer (75 mM KCl) for 20–30 min. After hypotonic treatment, cytospin was carried out as described above. After the slides were completely air-dried, cells were fixed in 4% PFA in PBS for 10 min on ice and subsequently permeabilized with RIPA (150 mM NaCl, 50 mM Tris–HCl, pH 8.0, 1% NP-40, 0.5% sodium deoxycholate, 0.1% SDS, 1 mM EDTA) buffer for 20 min. For RNase treatment, the slides were incubated with 100 μg/ml RNase A in 1× PBS for at least 1 h at 37°C. The sections were then washed three times with cold 1× PBS containing 0.05% Tween-20 (1× PBST) and prehybridized in hybridization buffer (50% formamide, 5× SSC, 5× Denhardt's solution, 25 mg/ml yeast RNA, 0.5 mg/ml salmon sperm DNA) for 1 h at 37°C. Hybridization was performed overnight at 37°C, and the PNA probe (PNA Bio Inc.) was used in the hybridization. The antisense probe (Cy3-GCGAGGAAAACTGAAAAAGG) was used to detect sense major satellite transcripts. After hybridization, slides were washed as follows: three times in [2× SSC, 50% formamide] at 39°C for 5 min; three times in 2× SSC at 39°C for 5 min each; 10 min in 1× SSC at room temperature, and once in 4× SSC at room temperature. The slides were then fixed again in [2% PFA in 0.1% Triton X-100, 1× PBS] for 5 min and washed three times with 1× PBST for 10 min each. DNA FISH with a sense probe (FAM-TTGCCATATTCCACGTCC from PNA Bio Inc.) was subsequently performed to detect major satellite DNA region, used according to the manufacturer's instructions. After washes, slides were subject to RNase A treatment by the incubation in 100 μg/ml RNase A in 1× PBST for 30 min at 37°C. Slides were washed three times in 1× PBS and dehydrated in ethanol series 5 min for each (70%, 85%, 100%). Slides were denatured at 85°C for 5 min in the presence of 50 μl of the hybridization buffer (60% formamide, 20 mM Tris–HCl, pH 7.4, 0.1 μg/ml salmon sperm DNA) containing the sense probe, and hybridization was performed in dark for 2 h at room temperature. The slides were then washed twice at 55–60°C for 10 min each in [2× SSC/0.1% Tween-20], stained with DAPI, and mounted with Vectashield (Vector Labs). Image capture and process were performed using the same methods as described above in the "immunofluorescence" section.

Combined immunofluorescence and DNA FISH

Hypotonic treatment and cytospin of cell suspensions from a 21–24 dpp testis were carried out as described above. After the slides were completely air-dried, cells were fixed in 4% PFA in 1× PBS for 10 min on ice, and subsequently, immunofluorescence on slides was performed as described above. Slides were probed with the indicated the following primary antibodies: human anti-centromere positive serum (Antibodies Inc. 15-235-0001, 1:200), sheep polyclonal anti-BUBR1 antibody (Abcam, ab28193, 1:100), mouse monoclonal anti-Hec1 antibody (Santa Cruz biotechnology Inc, sc-515550, 1:50), goat polyclonal anti-CENP-A antibody (Santa Cruz biotechnology Inc, sc-11278, 1:50), rabbit monoclonal anti-REC8 antibody (Abcam, ab192241, 1:50), and rabbit polyclonal anti-SGO1 antibody (Atlas antibodies, HPA035501, 1:50). This was followed by binding with Alexa 488- or 633-conjugated anti-mouse, anti-rabbit, anti-goat, anti-human, or anti-sheep IgG antibodies. After washes, slides were fixed again in 2% PFA in 0.1% Triton X-100/1× PBS for 5 min. Slides were further incubated in fresh Carnoy's fixative (3:1 ratio of methanol: acetic acid) at 4°C for 30 min, air-dried, aged for at least a day, and subject to performed DNA FISH with antisense probe for major satellite DNA region as described above.

Northern blot analysis

To enrich for the total RNA from purified spermatocyte, PicoPure™ RNA Isolation Kit (Thermo Fisher) was used according to the manufacturer's instructions. For Northern blot analysis, 0.5–1 μg of total RNA was separated on 1% denaturing agarose gel and transferred to Hybond™-N+ membranes (GE Healthcare). The oligonucleotides used to probe for major (mixture of Maj23 and Maj12) and minor (mixture of Min1, Min2, and Min3) satellite repeats, and PCR primers for generating 28S rRNA probe were designed based on previous reports (Cui & Tseng, 2004; Hsieh *et al*, 2011) and are listed in Appendix Table S1. Probes were 5′-end-labeled with [γ-^{32}P] ATP using T4 polynucleotide kinase (New England Biolabs). Prehybridization of the filters was carried out in 6× SSC, 0.2% SDS, and 5× Denhardt's solution. Hybridizations were performed in the same solution at 42°C, with addition of the denatured, labeled probes. After hybridization, the blots were subjected to stringent washes with 4× SSC, 0.2% SDS at 42°C four times for 10 min, and subsequently autoradiography using Storage Phosphor screens (GE Healthcare). Before re-probing, the membrane was washed with (boiling 1% SDS in water) and then let naturally cool to RT twice.

Constructs for ectopic expression of satellite RNAs

For ectopic expression of satellite RNAs, pCALNL-DsRed (Matsuda & Cepko, 2007), a gift from Connie Cepko (Addgene plasmid #13769), was used as the vector with a minor modification. The coding sequence of DsRed was excised with AgeI and NotI from pCALNL-DsRed, and blunt ended to obtain the empty vector (pCALNL). Major satellite sequences were obtained from pγsat (Addgene plasmid #39238), which contain 8 tandem repeats of mouse major satellite, as described previously (Lundgren *et al*, 2000). The major satellite sequence was excised with NotI and salI, blunt ended and cloned into pCALNL, and further sequenced to confirm that the vector and the insert are with correct orientation to express sense or antisense stand of major satellite repeats. For minor satellite repeats, the 7 tandem repeats of mouse minor satellite were amplified by PCR with the primers 5′-TTTTGGTACC-CATGGAAAATGATAAAAACC-3′ (with a KpnI-recognized site, underlined) and 5′-TTTTGAATTCCATCTAATATGTTCACAGTGTGG-3′ (with a EcoRI-recognized site, underlined). The amplified

fragment (s-min-7x) was then blunt ended and cloned into pCALNL- to generate pCALNL-s-min-7x. To produce antisense strand of minor satellite repeats, the 14 tandem repeats of minor satellite were excised with KpnI and sawI, blunt ended, and cloned into pCALNL, which was digested with Acc651 and blunt ended. To express 18S rRNA, the 1,870 bp rDNA sequence was amplified by PCR with the primers 5′-TTTGGTACCACCTGGTTGATCCTGCCAGG-3′ and 5′-TTTGGTACCTCAATCTGTCAATCCTGTCC-3′ (with a KpnI-recognized site, underlined). The amplified fragment was cloned into pCALNL.

For conditional activation of shRNA, pSico (Ventura *et al*, 2004), a gift from Tyler Jacks (Addgene plasmid #11578), was used as template with a minor modification: The coding sequence of EGFP was excised with AgeI and NotI from pSico, and replaced with the coding sequence of mCherry, which were amplified by PCR with the primers 5′-CGCTACCGGTCGCCACCATGGTGAGCAAGGGCGAGGAG-3′ (with a AgeI-recognized site, underlined) and 5′-TTATGCGGCCGTTACTTGTACAGCTCGTCCAT-3′ (with a NotI-recognized site, underlined). All shRNA oligo sequences are listed in Appendix Table S1. The construction of shRNA expression vector was according to the described previously (Ventura *et al*, 2004).

Sertoli-spermatogenic cell co-culture

The Sertoli-spermatogenic cell co-culture was carried out as previously described (Tres & Kierszenbaum, 1983, 1999; Marh *et al*, 2003). Testes were collected from 20 dpp mice, tunica albuginea was removed, and tissue was incubated with digestion buffer (0.5 mg/ml collagenase type IV, 0.05% and trypsin–EDTA in DMEM) for 10 min at 37°C, followed by pipetting to release the cells, and then added 10% volume of fetal bovine serum (FBS) to stop the reaction. Cells were washed twice with Eagle's Minimum Essential Medium (EMEM) containing 10% FBS, 4 mM glutamine, 1 mM sodium pyruvate, and 0.1 mM nonessential amino acids. Cells were seeded at 3×10^6 cells/ml in 24-well tissue plates and incubated 7–8 h to adhere to the well for use in further transfection. To transfect the indicated plasmids, Lipofectamine 3000 (Invitrogen) was used according to the manufacturer's instructions. The cells were incubated for 14–16 h and then switched the culture medium to the serum-free EMEM containing 5 μg/ml of insulin (Sigma), 5 μg/ml of transferrin (Sigma), 500 ng/ml of follicle-stimulating hormone (Sigma), 133 μIU/ml of growth hormone (human, recombinant; Sigma), 10 ng/ml of epidermal growth factor (R&D systems), 10 ng/ml of insulin-like growth factor 1(Sigma), 0.5 μM of retinoic acid (Sigma), 0.1 μM testosterone (Sigma), 4 mM glutamine, 1 mM sodium pyruvate, and 0.1 mM nonessential amino acids and antibiotics (100 U/ml of penicillin and 100 μg/ml of streptomycin). The cells were harvested after 50–54 h. To collect MIWI-expressing spermatocytes, cells were analyzed using a BD FACSAriaII according to GFP expression level and cell size. Sorted cells were collected by centrifugation at 500 *g* for 5 min and then subjected to further experiments.

RNA Immunoprecipitation and small RNA northern blot

Nuclei were prepared as described above and then resuspended in lysis buffer [50 mM Tris–HCl (PH 7.4), 2.5 mM $MgCl_2$, 100 mM KCl, 0.1% Nonidet P-40, 1× Complete proteinase inhibitor (Roche), 50 units/ml RNaseOUT (Invitrogen)]. The nuclear lysates were further passed through a 26-gauge needle 10 times on ice and rotated for 30 min. Cell debris was removed by centrifugation at 21,000 *g* for 30 min at 4°C. Immunoprecipitation was performed by adding the mouse monoclonal anti-MIWI antibody (Wako) to the nuclear extracts and incubated for 3 h at 4°C. Dynabeads Protein G (Invitrogen) were added to each IP sample and rotated for 1 h at 4°C. The beads were pelleted and washed six times with 0.5 ml of lysis buffer. Bound RNA in IP, as well as input RNA (1/10 of nuclear lysate) were isolated using TRIzol reagent (Invitrogen) according to the manufacturer's instructions. The immunoprecipitated RNA was separated on 12% polyacrylamide/8 M urea denaturing gels and transferred to Hybond™-N+ membranes (GE Healthcare). The oligonucleotides used to probe for piR major-a, piR major-b, piR major-c, piR major-as, piR-A, piR-E, and miR-16 are listed in the Appendix Table S1. Hybridization was performed as described above in the "Northern blot" section.

RNA pull-down assay

RNA pull-down assay was carried out as described previously (Hsieh *et al*, 2011). For *in vitro* synthesis of biotinylated transcripts corresponding to approximately one unit of the major and minor satellite repeats, templates were first generated by PCR using chimeric oligonucleotide primers that encompass T7 RNA polymerase promoter sequence (Appendix Table S1). Templates corresponding to partial 18S rRNA and *Gapdhs* (Glyceraldehyde-3-phosphate dehydrogenase, testis-specific) sequences that are similar lengths to the one and two repeat units of minor and major satellite repeats were used as controls. PCR products were cloned into pGEM-T easy vector (Promega) for further sequencing, and then, plasmids were amplified and digested by EcoRI and SpeI to obtain the DNA templates for *in vitro* transcription. In order to synthesize biotinylated transcripts, AmpliScribe™ T7-Flash™ Biotin-RNA Transcription Kit (EPICENTRE) was then used according to the manufacturer's instructions. 0.5 μg of the resulting biotinylated transcripts was mixed with 1 mg of 21–24 dpp testicular extracts that were prepared as described above. The Mg^{2+}-free lysis buffer [150 mM KCL, 25 mM Tris, pH 7.4, 5 mM EDTA, 0.5 mM DTT, 0.5% NP-40, 2 mM Na_3VO_4, 1 mM NaF, 1× Complete proteinase inhibitor (Roche), 50 units/ml RNaseOUT (Invitrogen)] was used to prevent RNA substrates from cleaved by Dicer (RNase III proteins) and MIWI (RNase H-like proteins). All steps of the pull-down assay were performed at 4°C. The supernatants were precleared with Dynabeads M-280 (Invitrogen), in the presence of SUPERase·In (0.05 U/ml) (Ambion) and yeast tRNA (25 μg/ml) (Sigma), for 1 h with rotation. After removing beads, 500 ng of *in vitro* transcribed biotinylated RNA was added to the supernatant and the mixture was further incubated for 1 h. The protein-biotinylated RNA complexes were recovered by addition of 30 μl Dynabeads M-280 (1 h incubation with rotation), and the bound complexes were washed four times with WCE buffer and subsequently analyzed by 4–15% SDS–PAGE and Western blot. Blots were probed with rabbit polyclonal anti-MIWI antibody (Cell Signaling), rabbit polyclonal anti-MILI antibody (Cell Signaling), rabbit polyclonal anti-GAPDH antibody (Sigma), rabbit monoclonal anti-PUM 1 antibody (Abcam), and rabbit polyclonal anti-Dicer antibody (Bethyl Laboratories, Inc.).

In vitro RNA processing assay

The *in vitro* RNA processing assay was carried out largely as described previously (Reuter *et al*, 2011), with the following modifications. *In vitro* synthesis of transcripts of the major and minor satellite repeats was performed as described above in the "RNA pull-down assay" section. Templates corresponding to partial 18S rRNA sequence of equivalent lengths to the one and two repeats of minor and major satellite repeats (162, 300, and 542 bp) were used as control. In order to synthesize target RNAs, AmpliScribe™ T7-Flash™ Transcription Kit (EPICENTRE) was used according to the manufacturer's instructions. Target RNAs were gel eluted from 6% urea-polyacrylamide gels and 5′-end labeled with [γ-^{32}P] ATP using T4 polynucleotide kinase (New England Biolabs). 10^6 Nuclei or whole-cell pellets from 21 to 24 dpp testes were resuspended in 10 μl slicer buffer [10 mM Tris–HCl pH 7.5, 100 mM KCl, 2 mM $MgCl_2$, 40 U RNaseOUT (Invitrogen)] for 15 min at 4°C, vortexed every 5 min, centrifuged at 20,000 *g* for 10 min, and collected the supernatants for nuage–nuclear fraction (N) and whole-cell extracts (T), respectively. To remove endogenous Dicer, immunodepletion was performed with 100 μl of whole-cell extracts. The supernatants were incubated with 2.5 μg mouse monoclonal anti-MIWI antibody (Wako) for 3 h at 4°C with gentle agitation and subsequently with the addition of Dynabeads Protein G (Invitrogen) for additional 1 h. Control depletions were performed using pre-immune mouse IgG. The Dicer- and IgG-depleted whole-cell extracts were obtained from collecting the supernatants of immunodepletion reactions.

To purify MIWI for cleavage assays, adult testes from 3xFLAG-tagged MIWI transgenic and wild-type mice (as a negative control) were used to perform immunoprecipitation using the same methods as described above in the "Immunoprecipitation" section. One entire testis was used to conduct two immunoprecipitation reactions by adding anti-FLAG M2 Magnetic beads (sigma, 15 μl/reaction) to the extracts and incubated for 3 h at 4°C. The beads were washed three times with 0.5 ml of lysis buffer and then resuspended in 10 μl slicer buffer for 30 min.

To prevent the major satellite substrates from targeting by the MIWI-piRNA complex, 25-nt complimentary 2′-o-methyl RNA oligo was first incubated with the RNA substrates for 30 min at RT before *in vitro* RNA processing reaction. The *in vitro* RNA processing reaction was performed in a thermoshaker (Eppendorf) for 2 min-1 h at 37°C (300 rpm). The RNA substrates were isolated using TRIzol reagent (Invitrogen). RNA was resolved by 8% Urea–PAGE. Gels were dried and exposed to Storage Phosphor screens (GE Healthcare).

Small RNA identification

The publicly available dataset that contains deep-sequencing of small RNAs after immunoprecipitation of MIWI from adult mouse testis [GSE19172] (Robine *et al*, 2009) was used to seek the potential piRNAs to target satellite transcripts. Bowtie (Langmead *et al*, 2009) was performed to align MIWI-immunoprecipitated small RNA-seq to satellite RNAs with up to 3 mismatches. According to previous studies (Reuter *et al*, 2011), the efficient cleavage of target RNAs by MIWI slicer activity is required for base pairing of nucleotides 2–22 of piRNAs. Potential piRNAs that fit this criterion were further confirmed by Northern blot analysis.

Nuclear run-on assay

The nuclear run-on assay was carried out as described previously (Hsieh *et al*, 2011). Purified spermatocytes were washed twice with ice-cold 1× PBS and collected by centrifugation (500 *g*, 5 min). Cell pellets were resuspended in 100 μl of lysis buffer (10 mM Tris–HCl, pH 7.4, 10 mM NaCl, 3 mM $MgCl_2$, 40 μg/ml Digitonin) per 10^6 cells. After 10-min incubation on ice, nuclei were then collected by centrifugation (500 *g*, 5 min) and washed with lysis buffer devoid of Digitonin. To perform run-on reactions, aliquots of nuclei were mixed with 25 μl of 2× reaction buffer (20 mM Tris–HCl pH 8.0, 5 mM $MgCl_2$, 200 mM KCl, 4 mM dithiothreitol, 4 mM each of ATP, CTP and GTP, 200 mM sucrose, and 20% glycerol) and 0.4 mM biotin-16-UTP (Roche) in a final volume of 50 μl at 29°C for 30 min. A total of 15 U of RNase-free DNaseI (Fermentas; Burlington, Ontario, Canada) and 1.5 μl 250 mM $CaCl_2$ were added, and the reaction mixture was incubated for an additional 10 min at 37°C. The nuclear run-on RNA and total RNA were then digested with DNase I (Ambion) to further remove contaminating genomic DNA. Biotinylated RNA was purified by Dynabeads M-280 (Invitrogen), a magnetic bead covalently linked to streptavidin. Dynabeads resuspended in binding buffer (10 mM Tris–HCl, pH 7.5, 1 mM EDTA, and 2 M NaCl) were mixed to an equal volume of run-on RNA and subjected a 2-h incubation at room temperature. Beads were separated by the magnetic apparatus and washed once with 500 μl 2× SSC-15% formamide for 10 min and twice with 1 ml 2× SSC for 5 min each. Random hexamer-primed cDNA was synthesized using Superscript II reverse transcriptase (Invitrogen) with 10 μl biotinylated RNA and 100 ng total RNA, and subsequently subjected to real-time PCR to assay for major and minor satellite RNA and 5.8S rRNA transcription rate. To ensure the efficiency of the reverse transcription, the intensities of PCR products were normalized to those of U5 snRNA (primers are listed in the Appendix Table S1).

Methylation-sensitive restriction analysis

Methylation-sensitive restriction analysis was carried out as previously described (Lei *et al*, 1996). Genomic DNA of purified spermatocytes was isolated using DNeasy Blood & Tissue Kit (QIAGEN). To examine the global methylation at pericentromeric and centromeric regions, genomic DNA was digested overnight with HpaII, a methyl-sensitive restriction enzyme (NEB) using 50 units of enzyme per 5 μg DNA. As control of digestion, another set of samples was digested with MspI, a methyl-sensitive restriction enzyme that recognizes the same target sequence as HpaII. An additional 10 units of enzyme was added the next morning to each sample to ensure complete digestion. For Southern blot analysis, 1 μg of purified DNA was separated on 1% agarose gel, transferred to Hybond™-N+ membrane, and hybridized to ^{32}P-labeled probes at 55 °C in hybridization buffer (5 × SSC, 2.5× Denhardt's solution, 0.1% SDS and 20 mg/ml sheared, denatured salmon sperm DNA) overnight. After hybridization, the blots were subjected to stringent washes with 2 × SSC/0.1% SDS at 42°C twice and then in 0.1 × SSC/0.1% SDS at 50°C twice, and subsequently autoradiography using Storage Phosphor screens (GE Healthcare). PCR primers for generating the *Gapdh* and LINE1 DNA probes are listed in the Appendix Table S1.

Immunoprecipitation

Total testis extracts from 22 to 24 dpp *Miwi* heterozygote or *Mov10l1*$^{f/-}$; *Stra8-Cre* line were pelleted and then washed twice in 1× PBS, and subsequently treated with lysis buffer (50 mM Tris–HCl (PH 7.4), 2.5 mM $MgCl_2$, 100 mM KCl, 0.1% Nonidet P-40, 1× Complete proteinase inhibitor (Roche), 50 units/ml RNaseOUT (Invitrogen)). The total testis lysates were further pass through 26-gauge needle 10 times on ice and rotated for 30 min. To remove endogenous RNA, 10 mg/ml RNase A was added in lysis buffer instead of 50 units/ml RNaseOUT. Cell debris was removed by centrifugation at 21,000 *g* for 30 min at 4°C. Immunoprecipitation was performed by adding mouse monoclonal anti-MIWI antibody (Wako) to the extracts and incubated for 3 h at 4°C. Dynabeads Protein G (Invitrogen) was added to each IP sample and rotated for 1 h at 4°C. The beads were pelleted and washed six times with 0.5 ml of lysis buffer, and boiled in 2× urea sample buffer dye for subsequent PAGE and immunoblotting analysis as described above. Blots were probed with rabbit polyclonal anti-MIWI antibody (Cell Signaling) and rabbit polyclonal anti-Dicer antibody (Bethyl Laboratories, Inc.). Rabbit polyclonal anti-TDRKH antibody (Proteintech) serves as a positive control. Rabbit polyclonal anti-Histone H3 antibody (Abcam) serves as a negative control.

Generation of MIWI and Dicer double knockout mice

To generate mice with MIWI and Dicer deficient in postnatal germ cells, we first bred *Miwi*$^{-/-}$ female mice with *Dicer*$^{flox/flox}$ male mice to obtain *Miwi*$^{+/-}$; *Dicer*$^{flox/+}$ mice. Male and female double-heterozygotes were intercrossed to generate *Miwi*$^{-/-}$; *Dicer*$^{flox/flox}$ female mice. To generate *Miwi*$^{+/-}$; *Dicer*$^{flox/+}$; *Stra8-Cre* male mice, *Miwi*$^{-/-}$; *Dicer*$^{flox/flox}$ female mice were crossed to *Stra8-Cre* transgenic mice, which expresses Cre recombinase at postnatal day 3. The *Miwi*$^{+/-}$; *Dicer*$^{flox/+}$; *Stra8-Cre* male mice were then crossed with *Miwi*$^{-/-}$; *Dicer*$^{flox/flox}$ female mice to generate *Miwi*$^{+/-}$; *Dicer*$^{flox/+}$; *Stra8-Cre*, *Miwi*$^{-/-}$; *Dicer*$^{flox/+}$; *Stra8-Cre*, *Miwi*$^{+/-}$; *Dicer*$^{flox/-}$; *Stra8-Cre,* and *Miwi*$^{-/-}$; *Dicer*$^{flox/-}$; *Stra8-Cre* mice.

Quantitative reserve transcription (RT) and real-time PCR

Total RNA from cells purified though FACS and immunoprecipitated RNA were isolated using TRIzol reagent (Invitrogen) according to manufacturer's instructions.

cDNA was synthesized by Superscript II reverse transcriptase (Invitrogen). Random hexamers and strand-specific primers were used to identify total and sense/antisense satellite transcripts, respectively. Primers for real-time PCR assays are listed in Appendix Table S1. Quantitative determination of the cDNA levels was done by real-time PCR using the Bio-Rad iTaq Universal SYBR Green Supermix system. All results represent the mean ± SD of at least three independent experiments.

5′ Rapid Amplification of cDNA Ends (5′ RACE)

Total RNA from cells purified though FACS was isolated using TRIzol reagent (Invitrogen) according to manufacturer's instructions. 5′-end cDNAs were prepared using SMARTer 5′/3′ kit (clontech) to specifically amplify the 5′ end of sense major satellite RNA. The amplified PCR products were cloned and sequenced for confirming their sequences. The gene-specific primers are listed in Appendix Table S1.

Mutating major satellite sequences for *In vitro* RNA processing assay

The specific deletion of monomers 2 and 3 of major satellite sequence (Wt, 118 nt) and the mismatch mutation (Mt-1-5) of approximately one repeat unit of major satellite sequence (308 nt) were created by PCR-based mutagenesis using Phusion High-Fidelity DNA PCR kit (NEB). The mutated sense major satellite transcripts include a deletion of 25-nt sequences for disrupting the base pairing with both of piR major-a and major-b (Δ25, 93 nt), a deletion of 10-nt sequences for disrupting the base pairing with 5′-end piR major-a (Δa, 108 nt), a deletion of 10-nt sequences for disrupting the base pairing with 5′-end piR major-b (Δb, 108 nt), and a deletion of 10-nt sequences for disrupting the base pairing with 3′-end piR major-a (Δc, 108 nt). Sequences for the primers are listed in Appendix Table S1.

RNase III and nuclease S1 digestion

Total RNA from purified spermatocyte was extracted using TRIzol reagent (Invitrogen). 0.5 μg of total RNA was added to RNase III reaction mix [1U RNase III (Ambion) and Ix reaction buffer] and further incubated for 1 h at 37°C. For nuclease S1 treatment, the same amount of total RNA was mixed with 1 U nuclease S1 (Invitrogen), 10× reaction buffer, and 50 mM NaCl and further incubated for 1 min at 37°C. The resulting RNA was isolated using TRIzol reagent (Invitrogen). RNA was resolved by 1% denaturing agarose gel and subjected to perform Northern blot as described above.

Data availability

The authors declare that there are no primary datasets and computer codes associated with this study.

Expanded View for this article is available online.

Acknowledgments
We thank Shangqin Guo for Dicer$^{f/f}$ mice and Watanabe Toshiaki for generation of 3XFLAG-tagged *Miwi* transgenic mice. We are grateful to members of the Lin laboratory for discussions. This work was supported by NIH R37HD42012 to H.L.

Author contributions
C-LH performed the experiments. JX conducted bioinformatics analysis. C-LH and HL designed the study and wrote the paper. HL supervised the study.

Conflict of interest
The authors declare that they have no conflict of interest.

References

Abdurashitov MA, Chernukhin VA, Gonchar DA, Degtyarev S (2009) GlaI digestion of mouse gamma-satellite DNA: study of primary structure and ACGT sites methylation. *BMC Genom* 10: 322

Aldrup-Macdonald ME, Sullivan BA (2014) The past, present, and future of human centromere genomics. *Genes (Basel)* 5: 33 – 50

Allshire RC, Karpen GH (2008) Epigenetic regulation of centromeric chromatin: old dogs, new tricks? *Nat Rev Genet* 9: 923 – 937

Almeida R, Buscaino A, Allshire RC (2006) Molecular biology: silencing unlimited. *Curr Biol* 16: R635 – R638

Aravin AA, Hannon GJ, Brennecke J (2007) The Piwi-piRNA pathway provides an adaptive defense in the transposon arms race. *Science* 318: 761 – 764

Aravin AA, Sachidanandam R, Bourc'his D, Schaefer C, Pezic D, Toth KF, Bestor T, Hannon GJ (2008) A piRNA pathway primed by individual transposons is linked to *de novo* DNA methylation in mice. *Mol Cell* 31: 785 – 799

Beyret E, Liu N, Lin H (2012) piRNA biogenesis during adult spermatogenesis in mice is independent of the ping-pong mechanism. *Cell Res* 22: 1429 – 1439

Bian Y, Zhou W, Zhao Y, Li X, Geng W, Hao R, Yang Q, Huang W (2011) High-dose siRNAs upregulate mouse Eri-1 at both transcription and posttranscription levels. *PLoS ONE* 6: e26466

Bouzinba-Segard H, Guais A, Francastel C (2006) Accumulation of small murine minor satellite transcripts leads to impaired centromeric architecture and function. *Proc Natl Acad Sci USA* 103: 8709 – 8714

Buhler M, Haas W, Gygi SP, Moazed D (2007) RNAi-dependent and -independent RNA turnover mechanisms contribute to heterochromatic gene silencing. *Cell* 129: 707 – 721

Caceres-Gutierrez R, Herrera LA (2017) Centromeric non-coding transcription: opening the black box of chromosomal instability? *Curr Genomics* 18: 227 – 235

Chan FL, Wong LH (2012) Transcription in the maintenance of centromere chromatin identity. *Nucleic Acids Res* 40: 11178 – 11188

Chen ES, Zhang K, Nicolas E, Cam HP, Zofall M, Grewal SI (2008) Cell cycle control of centromeric repeat transcription and heterochromatin assembly. *Nature* 451: 734 – 737

Clift D, Marston AL (2011) The role of shugoshin in meiotic chromosome segregation. *Cytogenet Genome Res* 133: 234 – 242

Cobb J, Miyaike M, Kikuchi A, Handel MA (1999) Meiotic events at the centromeric heterochromatin: histone H3 phosphorylation, topoisomerase II alpha localization and chromosome condensation. *Chromosoma* 108: 412 – 425

Cui C, Tseng H (2004) Estimation of ribosomal RNA transcription rate *in situ*. *Biotechniques* 36: 134 – 138

De La Fuente R, Baumann C, Viveiros MM (2015) ATRX contributes to epigenetic asymmetry and silencing of major satellite transcripts in the maternal genome of the mouse embryo. *Development* 142: 1806 – 1817

Deng W, Lin H (2002) Miwi, a murine homolog of piwi, encodes a cytoplasmic protein essential for spermatogenesis. *Dev Cell* 2: 819 – 830

Deng W, Tsao SW, Lucas JN, Leung CS, Cheung AL (2003) A new method for improving metaphase chromosome spreading. *Cytometry A* 51: 46 – 51

Eaker S, Pyle A, Cobb J, Handel MA (2001) Evidence for meiotic spindle checkpoint from analysis of spermatocytes from Robertsonian-chromosome heterozygous mice. *J Cell Sci* 114: 2953 – 2965

Ernst C, Odom DT, Kutter C (2017) The emergence of piRNAs against transposon invasion to preserve mammalian genome integrity. *Nat Commun* 8: 1411

Eymery A, Callanan M, Vourc'h C (2009a) The secret message of heterochromatin: new insights into the mechanisms and function of centromeric and pericentric repeat sequence transcription. *Int J Dev Biol* 53: 259 – 268

Eymery A, Horard B, El Atifi-Borel M, Fourel G, Berger F, Vitte AL, Van den Broeck A, Brambilla E, Fournier A, Callanan M *et al* (2009b) A transcriptomic analysis of human centromeric and pericentric sequences in normal and tumor cells. *Nucleic Acids Res* 37: 6340 – 6354

Falconer E, Chavez EA, Henderson A, Poon SS, McKinney S, Brown L, Huntsman DG, Lansdorp PM (2010) Identification of sister chromatids by DNA template strand sequences. *Nature* 463: 93 – 97

Ferri F, Bouzinba-Segard H, Velasco G, Hube F, Francastel C (2009) Non-coding murine centromeric transcripts associate with and potentiate Aurora B kinase. *Nucleic Acids Res* 37: 5071 – 5080

Fishel B, Amstutz H, Baum M, Carbon J, Clarke L (1988) Structural organization and functional analysis of centromeric DNA in the fission yeast Schizosaccharomyces pombe. *Mol Cell Biol* 8: 754 – 763

Frost RJ, Hamra FK, Richardson JA, Qi X, Bassel-Duby R, Olson EN (2010) MOV10L1 is necessary for protection of spermatocytes against retrotransposons by Piwi-interacting RNAs. *Proc Natl Acad Sci USA* 107: 11847 – 11852

Fukagawa T, Nogami M, Yoshikawa M, Ikeno M, Okazaki T, Takami Y, Nakayama T, Oshimura M (2004) Dicer is essential for formation of the heterochromatin structure in vertebrate cells. *Nat Cell Biol* 6: 784 – 791

Gent JI, Dawe RK (2012) RNA as a structural and regulatory component of the centromere. *Annu Rev Genet* 46: 443 – 453

Goetz P, Chandley AC, Speed RM (1984) Morphological and temporal sequence of meiotic prophase development at puberty in the male mouse. *J Cell Sci* 65: 249 – 263

Gorbsky GJ (2015) The spindle checkpoint and chromosome segregation in meiosis. *FEBS J* 282: 2471 – 2487

Gou LT, Dai P, Yang JH, Xue Y, Hu YP, Zhou Y, Kang JY, Wang X, Li H, Hua MM *et al* (2014) Pachytene piRNAs instruct massive mRNA elimination during late spermiogenesis. *Cell Res* 24: 680 – 700

Greenlee AR, Shiao MS, Snyder E, Buaas FW, Gu T, Stearns TM, Sharma M, Murchison EP, Puente GC, Braun RE (2012) Deregulated sex chromosome gene expression with male germ cell-specific loss of Dicer1. *PLoS ONE* 7: e46359

Grenfell AW, Heald R, Strzelecka M (2016) Mitotic noncoding RNA processing promotes kinetochore and spindle assembly in Xenopus. *J Cell Biol* 214: 133 – 141

Grivna ST, Beyret E, Wang Z, Lin H (2006a) A novel class of small RNAs in mouse spermatogenic cells. *Genes Dev* 20: 1709 – 1714

Grivna ST, Pyhtila B, Lin H (2006b) MIWI associates with translational machinery and PIWI-interacting RNAs (piRNAs) in regulating spermatogenesis. *Proc Natl Acad Sci USA* 103: 13415 – 13420

Hain KO, Colin DJ, Rastogi S, Allan LA, Clarke PR (2016) Prolonged mitotic arrest induces a caspase-dependent DNA damage response at telomeres that determines cell survival. *Sci Rep* 6: 26766

Hecht NB (1986) *Regulation of gene expression during mammalian spermatogenesis. In Experimental approaches to mammalian embryonic development*. Cambridge Cambridgeshire, New York: Cambridge University Press

Hilz S, Modzelewski AJ, Cohen PE, Grimson A (2016) The roles of microRNAs and siRNAs in mammalian spermatogenesis. *Development* 143: 3061 – 3073

Hsieh CL, Lin CL, Liu H, Chang YJ, Shih CJ, Zhong CZ, Lee SC, Tan BC (2011) WDHD1 modulates the post-transcriptional step of the centromeric silencing pathway. *Nucleic Acids Res* 39: 4048 – 4062

Huang C, Wang X, Liu X, Cao S, Shan G (2015) RNAi pathway participates in chromosome segregation in mammalian cells. *Cell Discov* 1: 15029

Joseph A, Mitchell AR, Miller OJ (1989) The organization of the mouse satellite DNA at centromeres. *Exp Cell Res* 183: 494 – 500

Kanellopoulou C, Muljo SA, Kung AL, Ganesan S, Drapkin R, Jenuwein T, Livingston DM, Rajewsky K (2005) Dicer-deficient mouse embryonic stem cells are defective in differentiation and centromeric silencing. *Genes Dev* 19: 489 – 501

Khalil AM, Driscoll DJ (2010) Epigenetic regulation of pericentromeric heterochromatin during mammalian meiosis. *Cytogenet Genome Res* 129: 280 – 289

Kishikawa T, Otsuka M, Yoshikawa T, Ohno M, Ijichi H, Koike K (2016) Satellite RNAs promote pancreatic oncogenic processes via the dysfunction of YBX1. *Nat Commun* 7: 13006

Koh CM (2013) Preparation of cells for microscopy using cytospin. *Methods Enzymol* 533: 235 – 240

Kojima-Kita K, Kuramochi-Miyagawa S, Nagamori I, Ogonuki N, Ogura A, Hasuwa H, Akazawa T, Inoue N, Nakano T (2016) MIWI2 as an effector of DNA methylation and gene silencing in embryonic male germ cells. *Cell Rep* 16: 2819 – 2828

Korhonen HM, Meikar O, Yadav RP, Papaioannou MD, Romero Y, Da Ros M, Herrera PL, Toppari J, Nef S, Kotaja N (2011) Dicer is required for haploid male germ cell differentiation in mice. *PLoS ONE* 6: e24821

Kotaja N, Bhattacharyya SN, Jaskiewicz L, Kimmins S, Parvinen M, Filipowicz W, Sassone-Corsi P (2006) The chromatoid body of male germ cells: similarity with processing bodies and presence of Dicer and microRNA pathway components. *Proc Natl Acad Sci USA* 103: 2647 – 2652

Kuramochi-Miyagawa S, Watanabe T, Gotoh K, Totoki Y, Toyoda A, Ikawa M, Asada N, Kojima K, Yamaguchi Y, Ijiri TW *et al* (2008) DNA methylation of retrotransposon genes is regulated by Piwi family members MILI and MIWI2 in murine fetal testes. *Genes Dev* 22: 908 – 917

Langmead B, Trapnell C, Pop M, Salzberg SL (2009) Ultrafast and memory-efficient alignment of short DNA sequences to the human genome. *Genome Biol* 10: R25

Lee J, Iwai T, Yokota T, Yamashita M (2003) Temporally and spatially selective loss of Rec8 protein from meiotic chromosomes during mammalian meiosis. *J Cell Sci* 116: 2781 – 2790

Lei H, Oh SP, Okano M, Juttermann R, Goss KA, Jaenisch R, Li E (1996) *De novo* DNA cytosine methyltransferase activities in mouse embryonic stem cells. *Development* 122: 3195 – 3205

Li X, Dawe RK (2009) Fused sister kinetochores initiate the reductional division in meiosis I. *Nat Cell Biol* 11: 1103 – 1108

Lundgren M, Chow CM, Sabbattini P, Georgiou A, Minaee S, Dillon N (2000) Transcription factor dosage affects changes in higher order chromatin structure associated with activation of a heterochromatic gene. *Cell* 103: 733 – 743

Marh J, Tres LL, Yamazaki Y, Yanagimachi R, Kierszenbaum AL (2003) Mouse round spermatids developed *in vitro* from preexisting spermatocytes can produce normal offspring by nuclear injection into *in vivo*-developed mature oocytes. *Biol Reprod* 69: 169 – 176

Matsuda T, Cepko CL (2007) Controlled expression of transgenes introduced by *in vivo* electroporation. *Proc Natl Acad Sci USA* 104: 1027 – 1032

Meikar O, Da Ros M, Korhonen H, Kotaja N (2011) Chromatoid body and small RNAs in male germ cells. *Reproduction* 142: 195 – 209

Moazed D (2009) Small RNAs in transcriptional gene silencing and genome defence. *Nature* 457: 413 – 420

Murchison EP, Partridge JF, Tam OH, Cheloufi S, Hannon GJ (2005) Characterization of Dicer-deficient murine embryonic stem cells. *Proc Natl Acad Sci USA* 102: 12135 – 12140

Musacchio A, Desai A (2017) A molecular view of kinetochore assembly and function. *Biology (Basel)* 6: 5

Nguyen-Chi M, Morello D (2011) RNA-binding proteins, RNA granules, and gametes: is unity strength? *Reproduction* 142: 803 – 817

Orban TI, Izaurralde E (2005) Decay of mRNAs targeted by RISC requires XRN1, the Ski complex, and the exosome. *RNA* 11: 459 – 469

Parra MT, Gomez R, Viera A, Llano E, Pendas AM, Rufas JS, Suja JA (2009) Sequential assembly of centromeric proteins in male mouse meiosis. *PLoS Genet* 5: e1000417

Patel J, Tan SL, Hartshorne GM, McAinsh AD (2015) Unique geometry of sister kinetochores in human oocytes during meiosis I may explain maternal age-associated increases in chromosomal abnormalities. *Biol Open* 5: 178 – 184

Potapova T, Gorbsky GJ (2017) The consequences of chromosome segregation errors in mitosis and meiosis. *Biology (Basel)* 6: 12

Print CG, Loveland KL (2000) Germ cell suicide: new insights into apoptosis during spermatogenesis. *BioEssays* 22: 423 – 430

Reuter M, Berninger P, Chuma S, Shah H, Hosokawa M, Funaya C, Antony C, Sachidanandam R, Pillai RS (2011) Miwi catalysis is required for piRNA amplification-independent LINE1 transposon silencing. *Nature* 480: 264 – 267

Robine N, Lau NC, Balla S, Jin Z, Okamura K, Kuramochi-Miyagawa S, Blower MD, Lai EC (2009) A broadly conserved pathway generates 3′UTR-directed primary piRNAs. *Curr Biol* 19: 2066 – 2076

Rosic S, Kohler F, Erhardt S (2014) Repetitive centromeric satellite RNA is essential for kinetochore formation and cell division. *J Cell Biol* 207: 335 – 349

Rudert F, Bronner S, Garnier JM, Dolle P (1995) Transcripts from opposite strands of gamma satellite DNA are differentially expressed during mouse development. *Mamm Genome* 6: 76 – 83

Saksouk N, Simboeck E, Dejardin J (2015) Constitutive heterochromatin formation and transcription in mammals. *Epigenetics Chromatin* 8: 3

Sarangapani KK, Duro E, Deng Y, Alves Fde L, Ye Q, Opoku KN, Ceto S, Rappsilber J, Corbett KD, Biggins S *et al* (2014) Sister kinetochores are mechanically fused during meiosis I in yeast. *Science* 346: 248 – 251

Shomper M, Lappa C, FitzHarris G (2014) Kinetochore microtubule establishment is defective in oocytes from aged mice. *Cell Cycle* 13: 1171 – 1179

Sinha Hikim AP, Swerdloff RS (1999) Hormonal and genetic control of germ cell apoptosis in the testis. *Rev Reprod* 4: 38 – 47

Sun SC, Kim NH (2012) Spindle assembly checkpoint and its regulators in meiosis. *Hum Reprod Update* 18: 60 – 72

Tanaka T, Hosokawa M, Vagin VV, Reuter M, Hayashi E, Mochizuki AL, Kitamura K, Yamanaka H, Kondoh G, Okawa K *et al* (2011) Tudor domain containing 7 (Tdrd7) is essential for dynamic ribonucleoprotein (RNP) remodeling of chromatoid bodies during spermatogenesis. *Proc Natl Acad Sci USA* 108: 10579 – 10584

Thomas MF, Abdul-Wajid S, Panduro M, Babiarz JE, Rajaram M, Woodruff P, Lanier LL, Heissmeyer V, Ansel KM (2012) Eri1 regulates microRNA homeostasis and mouse lymphocyte development and antiviral function. *Blood* 120: 130 – 142

Thomas MF, L'Etoile ND, Ansel KM (2014) Eri1: a conserved enzyme at the crossroads of multiple RNA-processing pathways. *Trends Genet* 30: 298 – 307

Thomson T, Lin H (2009) The biogenesis and function of PIWI proteins and piRNAs: progress and prospect. *Annu Rev Cell Dev Biol* 25: 355 – 376

Ting DT, Lipson D, Paul S, Brannigan BW, Akhavanfard S, Coffman EJ, Contino G, Deshpande V, Iafrate AJ, Letovsky S *et al* (2011) Aberrant overexpression of satellite repeats in pancreatic and other epithelial cancers. *Science* 331: 593 – 596

Tres LL, Kierszenbaum AL (1983) Viability of rat spermatogenic cells *in vitro* is facilitated by their coculture with Sertoli cells in serum-free hormone-supplemented medium. *Proc Natl Acad Sci USA* 80: 3377 – 3381

Tres LL, Kierszenbaum AL (1999) Cell death patterns of the rat spermatogonial cell progeny induced by sertoli cell geometric changes and Fas (CD95) agonist. *Dev Dyn* 214: 361 – 371

Velazquez Camacho O, Galan C, Swist-Rosowska K, Ching R, Gamalinda M, Karabiber F, De La Rosa-Velazquez I, Engist B, Koschorz B, Shukeir N *et al* (2017) Major satellite repeat RNA stabilize heterochromatin retention of Suv39 h enzymes by RNA-nucleosome association and RNA:DNA hybrid formation. *Elife* 6: e25293

Ventura A, Meissner A, Dillon CP, McManus M, Sharp PA, Van Parijs L, Jaenisch R, Jacks T (2004) Cre-lox-regulated conditional RNA interference from transgenes. *Proc Natl Acad Sci USA* 101: 10380 – 10385

Vermeulen A, Behlen L, Reynolds A, Wolfson A, Marshall WS, Karpilow J, Khvorova A (2005) The contributions of dsRNA structure to Dicer specificity and efficiency. *RNA* 11: 674 – 682

Vissel B, Choo KH (1989) Mouse major (gamma) satellite DNA is highly conserved and organized into extremely long tandem arrays: implications for recombination between nonhomologous chromosomes. *Genomics* 5: 407 – 414

Vourekas A, Zheng Q, Alexiou P, Maragkakis M, Kirino Y, Gregory BD, Mourelatos Z (2012) Mili and Miwi target RNA repertoire reveals piRNA biogenesis and function of Miwi in spermiogenesis. *Nat Struct Mol Biol* 19: 773 – 781

Wang SW, Stevenson AL, Kearsey SE, Watt S, Bahler J (2008) Global role for polyadenylation-assisted nuclear RNA degradation in posttranscriptional gene silencing. *Mol Cell Biol* 28: 656 – 665

Watanabe Y (2004) Modifying sister chromatid cohesion for meiosis. *J Cell Sci* 117: 4017 – 4023

Watanabe Y (2012) Geometry and force behind kinetochore orientation: lessons from meiosis. *Nat Rev Mol Cell Biol* 13: 370 – 382

Watanabe T, Lin H (2014) Posttranscriptional regulation of gene expression by Piwi proteins and piRNAs. *Mol Cell* 56: 18 – 27

Watanabe T, Cheng EC, Zhong M, Lin H (2015) Retrotransposons and pseudogenes regulate mRNAs and lncRNAs via the piRNA pathway in the germline. *Genome Res* 25: 368 – 380

Wong AK, Rattner JB (1988) Sequence organization and cytological localization of the minor satellite of mouse. *Nucleic Acids Res* 16: 11645 – 11661

Yamagishi Y, Sakuno T, Goto Y, Watanabe Y (2014) Kinetochore composition and its function: lessons from yeasts. *FEMS Microbiol Rev* 38: 185 – 200

Zhang P, Kang JY, Gou LT, Wang J, Xue Y, Skogerboe G, Dai P, Huang DW, Chen R, Fu XD *et al* (2015) MIWI and piRNA-mediated cleavage of messenger RNAs in mouse testes. *Cell Res* 25: 193 – 207

Zheng K, Wang PJ (2012) Blockade of pachytene piRNA biogenesis reveals a novel requirement for maintaining post-meiotic germline genome integrity. *PLoS Genet* 8: e1003038

Zielinska AP, Holubcova Z, Blayney M, Elder K, Schuh M (2015) Sister kinetochore splitting and precocious disintegration of bivalents could explain the maternal age effect. *Elife* 4: e11389

